Copy of chapter from AAPM Summer School Proceedings:

Hogstrom, K.R., Antolak J.A., Kudchadker R.J., Ma C.-M. C., and Leavitt D.D. Modulated electron therapy. In: J Palta and R. Mackie (eds). Intensity Modulated Radiation Therapy, The State of the Art: Proceedings of the 2003 AAPM Summer School, pp. 749-786, Madison: Medical Physics Publishing, Madison, 2003.

Modulated Electron Therapy

Kenneth R. Hogstrom, Ph.D.[1], John A. Antolak, Ph.D.[1], Rajat J. Kudchadker, Ph.D.[1], C.-M. Charlie Ma, Ph.D.[2], and Dennis D. Leavitt, Ph.D.[3]
[1]Department of Radiation Physics
The University of Texas M.D. Anderson Cancer Center
Houston, Texas
[2]Department of Radiation Oncology
Fox Chase Cancer Center
Philadelphia, Pennsylvania
[3]Department of Radiation Oncology
University of Utah School of Medicine
Salt Lake City, Utah

Introduction

Radiation therapy has recently progressed to the extent that the delivery of complex, computer-controlled therapy has become more acceptable in radiation oncology practice. Although such sophistication has been accepted for at least four decades for

proton, pion, and heavy-ion therapy, the routine availability and utilization of conformal, intensity-modulated photon therapy has only recently occurred. Its acceptance has presented the opportunity to utilize modulated electron therapy (MET), which is capable of delivering highly conformal treatments to superficial targets. The high surface dose and minimal exit dose of electron therapy offers advantages over photon therapy for superficial targets. The rapid fall-off of the electron dose beyond the treatment volume can help reduce the dose to distal healthy tissues in the treatment of superficial tumors, such as those in the breast and head and neck regions.

The purpose of this chapter is to introduce the clinical medical physicist to the principles of modulated electron therapy, which undoubtedly will become an important tool for radiation therapy over the next decade.

Electron conformal therapy (ECT) is defined as the use of one or more electron beams for the following purposes: (1) containing the planning target volume (PTV) in the 90% (of given dose) dose surface; (2) achieving as homogeneous a dose as possible (e.g., 90% to 100%) or a prescribed heterogeneous dose distribution to the PTV; and (3) delivering a minimal dose to underlying critical structures and normal tissue. MET is defined as electron conformal therapy achieved through energy modulation and/or intensity modulation of the incident electron beam(s).

In MET, the energy and intensity of the incident electron beam are modulated in the plane perpendicular to the central axis of the electron beam. The beam intensity of an electron field can be modulated to improve the lateral dose conformity within the target volume, and different electron energies can be used to improve the dose conformity in the depth direction. Energy modulation can be achieved in either continuous or finite steps. Presently, there is no technology that allows the incident beam to have its energy spatially modulated in real time; therefore, electron energy is modulated by one of two methods. In the first method, energy modulation is achieved using electron bolus, which modulates the electron range in the patient by varying the bolus thickness across the beam. Because bolus thickness can be manufactured with 1 mm accuracy or better, the equivalent energy modulation is in steps of 0.2 MeV or less. In the second method, the patient is irradiated using multiple electron beams of differing energy. On conventional linear accelerators, energies are spaced at intervals ranging from approximately 1.5 to 4.0 MeV, corresponding to a 7- to 20-mm increment in beam penetration in unit density tissue. Beam intensity can be modulated using either a multileaf collimator (MLC) or multiple field cutouts. Three variations of energy and intensity modulation, namely, bolus ECT, segmented-field ECT, and intensity-modulated electron therapy (IMET), will be discussed in this chapter. The advantages and disadvantages of these variations will be discussed. Also, we will present how MET can be used to deliver electron arc therapy. Last, we will introduce the potential for mixed-beam therapy using MET. Our discussions will be limited to electron-beam energies currently available (6 to 25 MeV). MET for deep-seated tumors will not be discussed because it requires electron-beam energies substantially greater than 25 MeV, which are not commonly available.

MET has the same types of issues that intensity-modulated x-ray therapy (IMXT) does, namely, treatment planning, dose calculation, treatment delivery, quality

assurance, and clinical utility. Each of these issues will be discussed for the various types of MET reviewed in this paper.

Bolus Electron Conformal Therapy

Electron bolus has been defined as

> a specifically shaped material that is nearly tissue equivalent; it is normally placed either in direct contact with the patient's skin surface, close to the patient's surface, or inside a body cavity. This material is designed to provide extra scattering or energy degradation of the electron beam. Its purpose is to shape the dose distribution to conform to the target volume or to provide a more uniform dose inside the target volume.
>
> (Hogstrom 1992)

Bolus has been designed and used for many years to conform the fall-off of the electron beam dose distribution (e.g., the 90% dose surface) to the distal surface of the target volume. However, not until the work of Low et al. (1992) was the bolus designed to account for not only energy loss but also the effects of multiple Coulomb scattering of the electrons.

Treatment Planning

Low et al. (1992) designed bolus along fan lines emanating from the virtual electron source. As shown in figure 1, the initial design of the bolus, referred to as "creation," determined the bolus thickness along each fan-line that fell within the uniform portion of the electron beam. The thickness was designed so that when added to the depth of the distal PTV surface, it equaled the therapeutic depth (R_{90}). The resulting dose distribution was calculated using the three-dimensional (3-D) implementation of the Hogstrom pencil-beam algorithm (Hogstrom, Mills, and Almond 1981; Starkschall et al. 1991b). Due to effects of multiple Coulomb scattering, the bolus shape required modification. This was accomplished by various operators that smoothed the bolus proximal surface to homogenize PTV dose and that added or subtracted bolus material to make small adjustments necessary to conform the 90% isodose surface to the PTV. During this process, the bolus was extended laterally to be sufficiently outside the beam aperture to intercept essentially all electrons in the penumbra. This forward planning approach was implemented into the The University of Texas M. D. Anderson Cancer Center treatment-planning system, COPPERPlan (Starkschall et al. 1991a, 1994).

Treatment Delivery

Once the bolus is designed, the next step in the planning and delivery process is its fabrication. This was accomplished by milling a block of machineable wax using a

tabletop milling machine (Antolak et al. 1994; Low et al. 1995). The machineable wax has a linear stopping and linear scattering power similar to that of polyethylene (Low and Hogstrom 1994). The distal and proximal surfaces of the bolus were milled to the dimensions for the bolus provided by the treatment planning system. The distal surface was milled to match the patient's skin surface, and the proximal surface was milled to provide the conformal dose distribution. Studies by Bawiec (1994) showed that the milling process was sufficiently accurate. Experience showed, however, that the milling process using a table-top milling machine took too much time to be practical as a long-term clinical solution. Larger milling machines better suited for this process are not likely to be available to most radiation oncology centers; therefore, the M. D. Anderson Cancer Center clinic presently uses a bolus milling service (.decimal, Sanford, FL), which receives an electronic file of the bolus, mills it, and provides it to the institution the next day via overnight mail. Figure 2 shows a bolus milled for use on a patient with head and neck cancer.

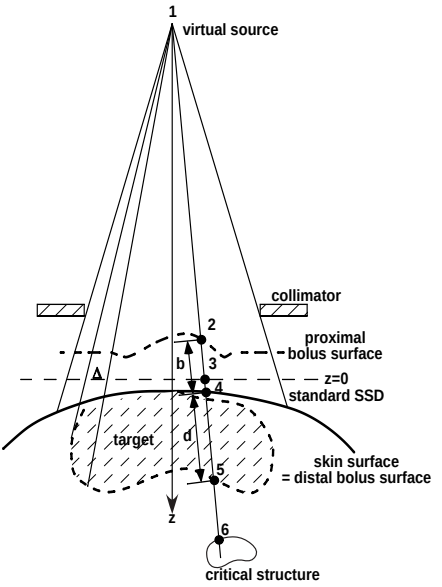

Figure 1. Sketch illustrating the fan geometry and design elements of the bolus design system. The design elements are illustrated through the representation of one fan line, on which points 1 through 6 are drawn. Point 1 represents the virtual electron source; points 2 through 6, the intersections of the fan line with the proximal bolus surface, the standard SSD plane, the proximal patient surface, the distal target volume surface, and the proximal critical structure surface, respectively. Bolus thickness, initially estimated by $b = R_{90}$-d, is modified to account for electron scatter and rate of energy loss in the bolus and patient. [Reprinted from *Medical Physics*, vol 19, D. A. Low, G. Starkschall, S. W. Bujnowski, L. L. Wang, and K. R. Hogstrom, "Electron bolus design for radiotherapy treatment planning: Bolus design algorithms," pp. 115–124. © 1992, with permission from AAPM.]

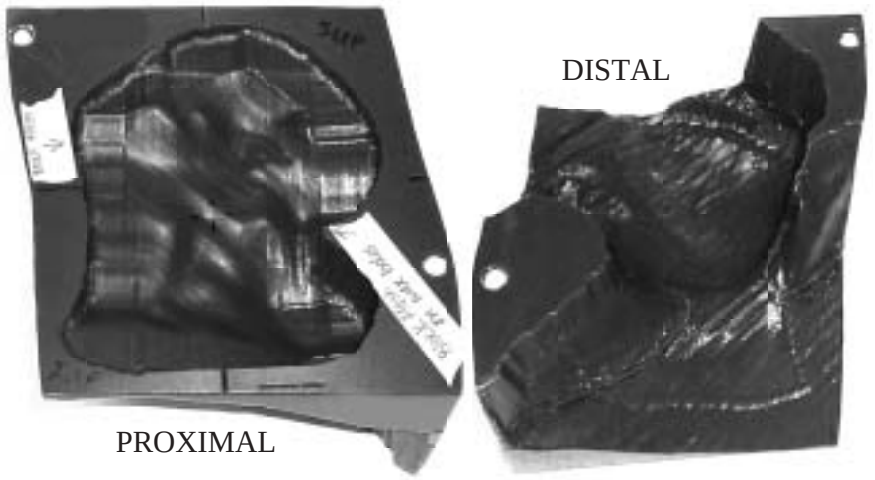

Figure 2. Custom electron bolus fabricated from machineable wax for head and neck treatment. The distal side is designed to match the patient's skin surface, and the proximal side is designed to modulate the penetration of the electron beam to match the PTV.

Quality Assurance

Bolus quality assurance is required prior to the bolus use. The bolus manufacturer assures that the milling process was accurate, but this is inadequate to verify the proper positioning of the bolus on the patient and resulting dose to the patient. Positioning and dose are verified by placing the bolus on the patient, performing a planning computed tomography (CT) scan, calculating the dose with the bolus in place using the appropriate beam parameters, and verifying that the resulting dose distribution is consistent with that originally designed. Figure 3 demonstrates this in a case in which a patient was treated using an electron bolus for a posterior wall sarcoma (Low et al. 1995).

Clinical Utility

The electron bolus has been clinically used primarily to treat postmastectomy chest wall and head and neck. In chest wall irradiation, the primary purpose of the electron bolus has been to minimize dose to the lung and heart. When treating the chest wall with electrons, surgical defects can often result in the chest wall thickness being highly irregular. Bolus can even the thickness, sparing considerable lung tissue. Alternatively, to spare lung, the chest wall is often irradiated using tangent photon beams that are abutted to an electron internal mammary chain (IMC) field. Such treatment is not as effective as bolus electron conformal therapy in cases in which disease at the IMC-chest wall field border is either known or highly likely or in which the anatomy of the

chest wall is highly distorted owing to surgery (Perkins et al. 2001). Figure 4 compares a bolus plan with a treatment plan achievable by the conventional technique using tangent photon fields matched to an electron IMC field. The bolus plan produces a significantly more uniform dose in the abutted region where the cancer had recurred.

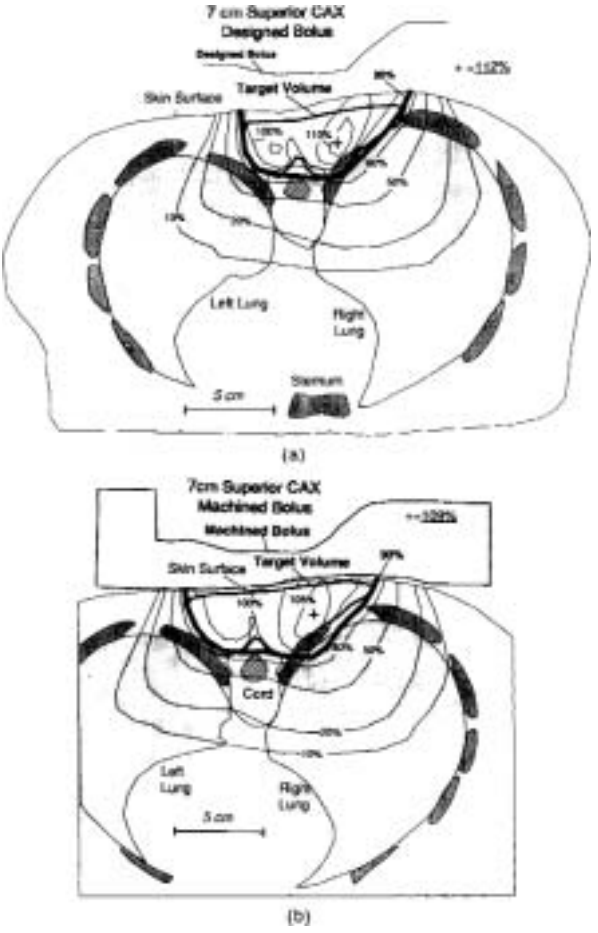

Figure 3. Example of quality assurance of bolus ECT for patient treatment of the paraspinal muscles. Anatomic structures, target volume, and the electron-beam isodose curves are superimposed on the transverse plane lying 7 cm superior to the central axis of the beam. (a) The treatment plan with the designed bolus. (b) The treatment plan for the CT scan with the bolus placed on the patient in treatment position. [Reprinted from *International Journal of Radiation Oncology Biology Physics*, vol 33, D. A. Low, G. Starkschall, N. E. Sherman, S. W. Bujnowski, J. R. Ewton, and K. R. Hogstrom, "Computer-aided design and fabrication of an electron bolus for treatment of the paraspinal muscles," pp. 1127–1138. © 1995, with permission from Elsevier.]

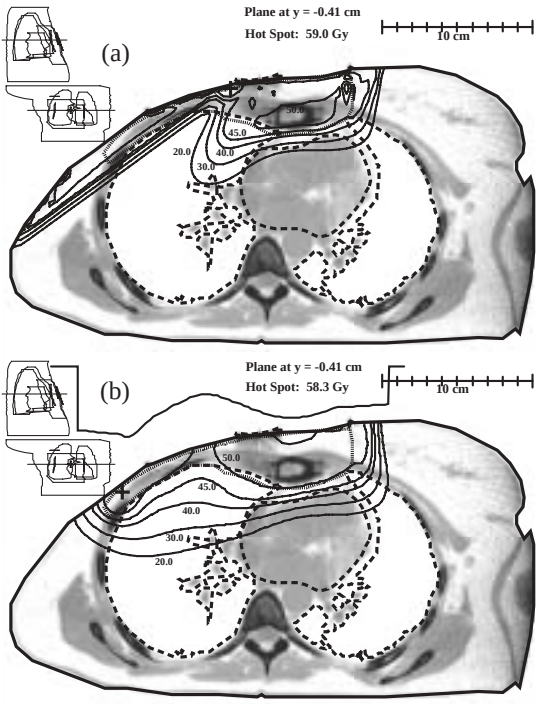

Figure 4. (a) Isodose curves (Gy) using standard tangent-IMC technique for a patient with a lesion in the right IMC area, with extension into the chest wall soft tissues. A dose of 50 Gy was prescribed to 100% of the given dose, using 12 MeV electrons for the IMC field, and the electron-field edge was matched to the medial tangent field edge on the patient's skin surface. The 45 Gy isodose line covers the target volume, except for the cold triangle directly beneath the junction line, an area of known disease. (b) Isodose curves (Gy) using the bolus ECT technique for the same patient. A dose of 50 Gy was prescribed to 100% of the given dose, using 16 MeV electrons, and the bolus was designed to deliver 90% of the given dose to the target volume. [Reprinted from *International Journal of Radiation Oncology Biology Physics*, vol 51, G. H. Perkins, M. D. McNeese, J. A. Antolak, T. A. Buchholz, E. A. Strom, and K. R. Hogstrom, "A custom three-dimensional electron bolus technique for optimization of postmastectomy irradiation," pp. 1142–1151. © 2001, with permission from Elsevier.]

Electron therapy in the head and neck is useful for sparing critical structures, such as the spinal cord, brain, and salivary glands. The use of electron beams in the head and neck can be further improved by using bolus conformal therapy. This is particularly true for PTVs that extend sufficiently inferiorly to overlay the spinal cord in the neck or superiorly to overlay brain tissue. The latter is exemplified in figure 5, which shows the PTV for a patient treated for a carcinoma of the left parotid gland. Figure 6 illustrates how the 90% dose surface conforms to the PTV in the same transverse planes as shown in figure 5. Figure 7 compares the dose-volume histogram (DVH) for

the custom bolus treatment plan with the DVH for an alternative method of treating the patient using two separate fields of differing energy (a 20 MeV superior field and a 12 MeV inferior field). The bolus conformal plan improves coverage of the PTV and gives lower doses to the spine and brain.

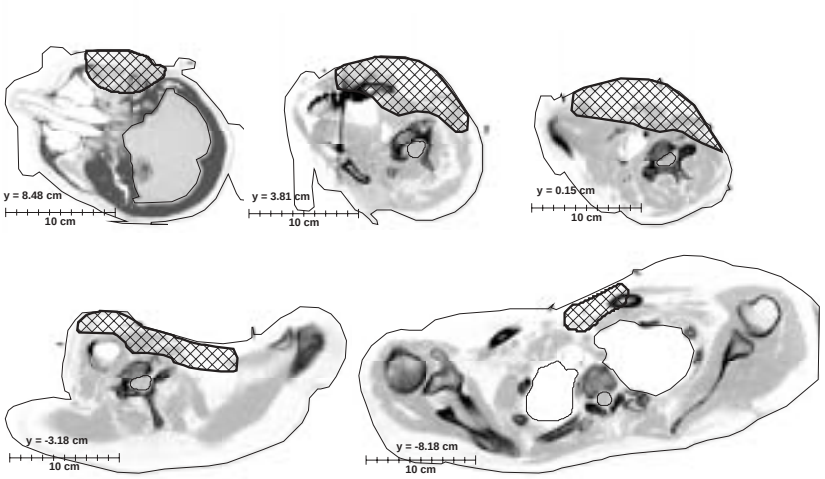

Figure 5. Transverse CT images (gray scale inverted for clarity) showing the location, depth, and shape of the parotid PTV (cross-hatched) at various levels. The maximum depth of the PTV is such that 20 MeV electrons were required for the bolus ECT treatment plan (Kudchadker et al. 2002a).

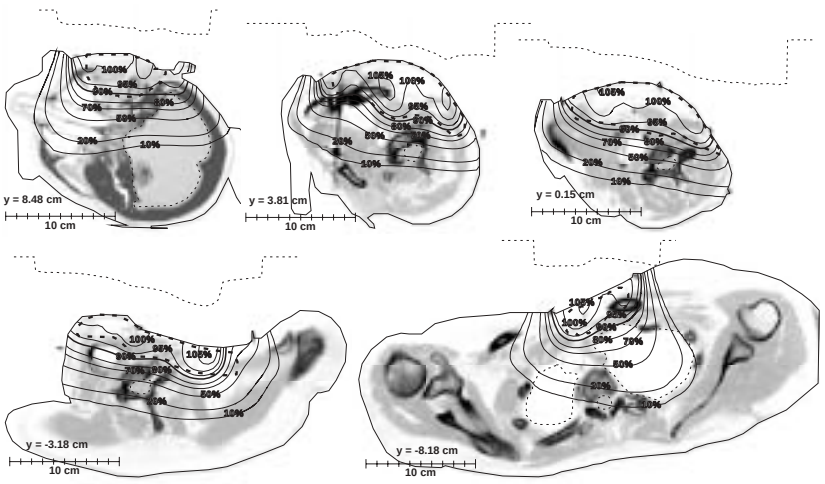

Figure 6. Dose distributions superimposed on transverse CT images from figure 5, illustrating how the bolus ECT treatment plan is able to conform the 90% isodose line to the PTV (dashed line) (Kudchadker et al. 2002a).

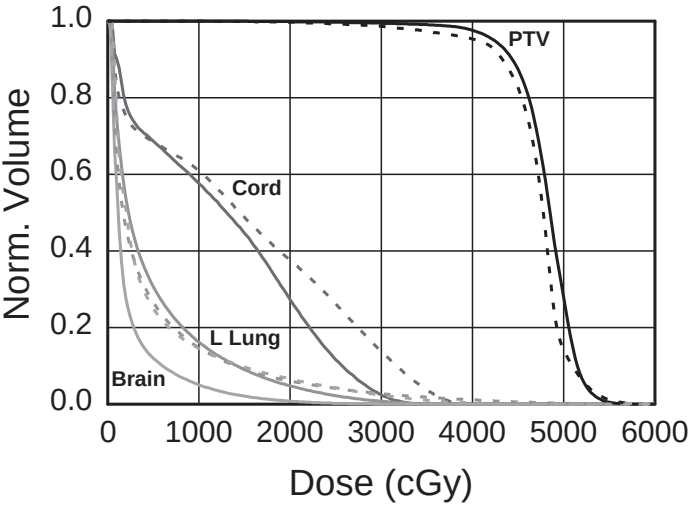

Figure 7. Dose-volume histograms for the PTV, spinal cord, left lung, and brain for the bolus ECT treatment plan shown in figure 6 (solid line) and a two-field plan with 20 MeV electrons superiorly and 12 MeV electrons inferiorly (dashed line) (Kudchadker et al. 2002a).

After planning bolus conformal therapy for many patients, Kudchadker et al. (2002b) observed that the irregular surface of the bolus increased the inhomogeneity of dose from a 10% variation (90% to 100%) in water (without bolus) to as much as a 20% variation (90% to 110%) in the patient (with bolus). This is illustrated in figure 8a, which shows the coronal plane dose distribution for a patient treated for carcinoma of the right buccal mucosa. Kudchadker et al. (2002b) showed that dose homogeneity could be restored by moderately modulating the intensity of the incident electron beam. Figure 8b shows the coronal dose distribution with intensity modulation, and the DVH comparison in figure 8c shows that the dose difference between 90% and 10% PTV coverage is reduced from 15% for the bolus plan to 9% for the bolus with the intensity-modulated plan. Figure 8d shows the relatively small amount of intensity modulation required for such a treatment.

The technique of bolus conformal therapy is relatively mature compared with the more recent MET techniques discussed below. Patients have been treated using bolus ECT technology for more than 10 years at M. D. Anderson, where its use has been demonstrated largely for breast and head and neck cancers. The treatment technique requires no modification to the electron treatment machine, and bolus fabrication with 1-day service is commercially available. A quality assurance process is well documented, and dose can be calculated using the pencil-beam dose algorithms presently available in 3-D treatment planning systems. The widespread use of bolus conformal therapy would require only the transfer of bolus design technology (Low et al. 1992) to commercial treatment planning systems.

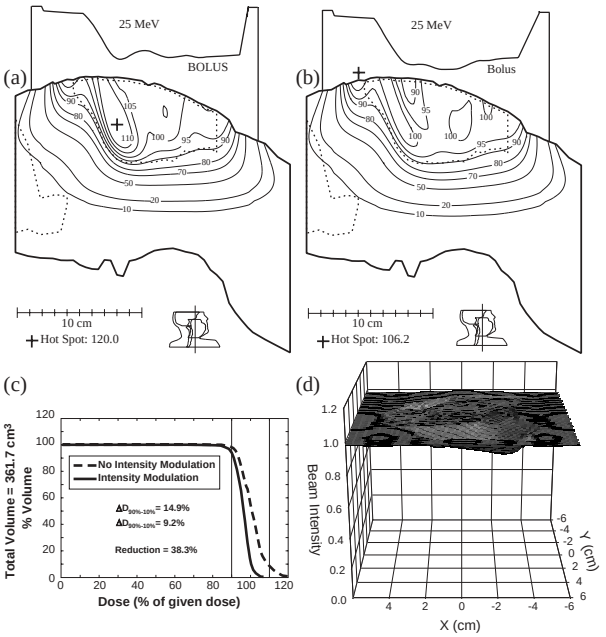

Figure 8. Bolus ECT dose distributions in a coronal plane are compared. Bolus ECT is planned with no intensity modulation (a), and with added intensity modulation (b). The treatment plans were designed to have the 90% isodose line cover the PTV (squamous cell carcinoma of the right buccal mucosa) and to deliver minimal dose to brain and other critical structures. The dotted lines demarcate the PTV and the base of brain. Note decrease in hot spot from 120% to 106%. (c) DVH for PTV comparing treatment plans with and without intensity modulation. (d) Beam intensity map required for the intensity-modulated bolus ECT plan. [Reprinted from *International Journal of Radiation Oncology Biology Physics*, vol 53, R. J. Kudchadker, K. R. Hogstrom, A. S. Garden, M. D. McNeese, R. A. Boyd, and J. A. Antolak, "Electron conformal radiotherapy using bolus and intensity modulation," pp. 1023–1037. © 2002, with permission from Elsevier.]

Segmented-Field Electron Conformal Therapy

Segmented-field ECT is defined here as the utilization of multiple abutted electron fields, each having a common virtual source position but each having its own energy and weight, so as to conform the therapeutic dose surface (e.g., 90% of given dose) to the PTV. An example of segmented-field ECT (Zackrisson and Karlsson 1996) for postmastectomy chest wall irradiation is illustrated in figure 9. Segmented-field ECT can be applied to treatment of the parotid gland, improving upon the crude example in the previous section, where the superior segment (parotid) of the field was planned with a greater energy and the inferior segment (neck nodes) with a lesser energy so as to protect the spinal cord.

Treatment Planning

Segmented-field ECT can be planned using existing technology, namely, using an appropriate 3-D treatment planning system. The 3-D treatment planning system needs a sufficiently accurate dose calculation (e.g., the Hogstrom pencil-beam algorithm) and the ability to model beam edges accurately. Unfortunately, manufacturers do not provide a key tool, a beam's eye view of PTV depth (Starkschall et al. 1994), which could be useful for manually segmenting the field. Figure 10 shows an example of such a tool and how it could be used to manually segment the field into smaller fields of differing energy and weights. It should be possible to automate this process by incorporating some basic rules of abutting electron fields into an algorithm.

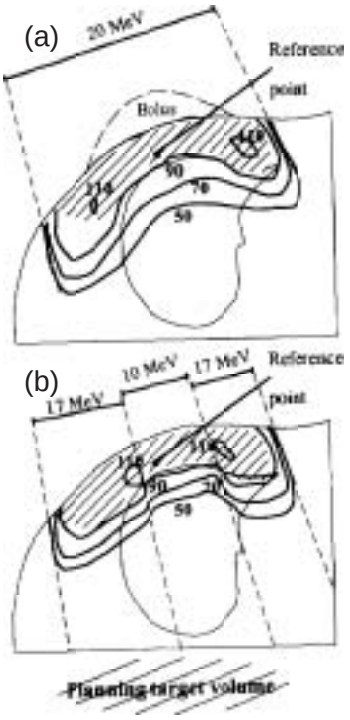

Figure 9. Comparison of bolus ECT with segmented-field ECT treatment plan for irradiation of the thoracic wall and the IMC after radical mastectomy. Dose distribution is shown in a transverse section for (a) the bolus ECT plan using 20 MeV electrons from a single portal and (b) the segmented-field ECT plan, which has three segments with a common isocenter. The segmented-field ECT plan uses 10 MeV electrons for the central segment and 17 MeV electrons for the medial and lateral segments. The reference point was used for dose normalization. [Reprinted from *Radiotherapy & Oncology*, vol 39, B. Zackrisson and M. Karlsson. "Matching of electron beams for conformal therapy of target volumes at moderate depths," pp. 261–270. © 1996, with permission from Elsevier.]

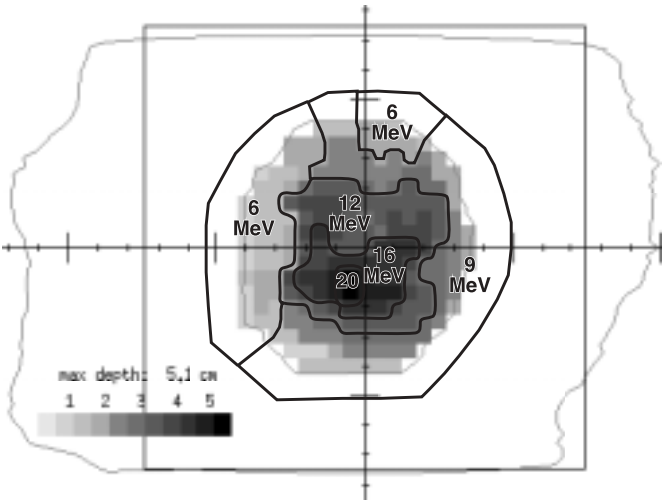

Figure 10. Potential of beam's eye view depth-display tool for segmented-field ECT. Gray levels are used to map the depth of the distal PTV surface. The depth map is used to segment the field into multiple beams of differing energy, selecting from the five beam energies available on the radiotherapy accelerator. In this example, for initial energy segmentation, the minimum beam energy whose therapeutic depth of the broad beam (R_{90}) exceeds the depth of the PTV is selected.

Treatment Delivery

The delivery of segmented-field ECT remains an issue. Currently, the only practical way to deliver segmented fields is to fabricate multiple Cerrobend® inserts, one for each beam energy, with each insert having possibly multiple apertures. For this to work best, the Cerrobend edges should probably be fabricated with divergent edges. An alternative is to utilize an MLC. Zackrisson and Karlsson (1996) demonstrated that the x-ray MLC on a Scanditronix MM50 racetrack microtron can serve also as an electron MLC (eMLC). The electron penumbra remains sufficiently small for its utilization because (1) the downstream edge of the MLC is only 35 cm above isocenter, (2) the head of the machine is filled with helium, (3) the virtual source is small owing to the utilization of a scanned beam, and (4) the leaves are doubly focused. X-ray MLCs from other manufacturers are not sufficient to be used as eMLCs because (1) the downstream edges are too far from isocenter, (2) the heads of the machines are filled with air, and (3) the virtual sources are large because the beams are broadened by dual scattering foil systems. This is illustrated in figure 11, using data from Klein (1998). In this case, the penumbra from the Varian MLC was so great that it was not possible to segment beams in such a way as to track closely the sharp gradient in the distal edge of the anterior portion of the PTV for a parotid case. Potential solutions to

this issue are to redesign the treatment head (Karlsson, Karlsson, and Ma 1999; Karlsson and Karlsson 2002) or to develop eMLCs that replace Cerrobend inserts (Lee, Jiang, and Ma 2000; Ma et al. 2000b) or the entire applicator system (Antolak, Boyd, and Hogstrom 2002; Boyd, Antolak, and Hogstrom 2002).

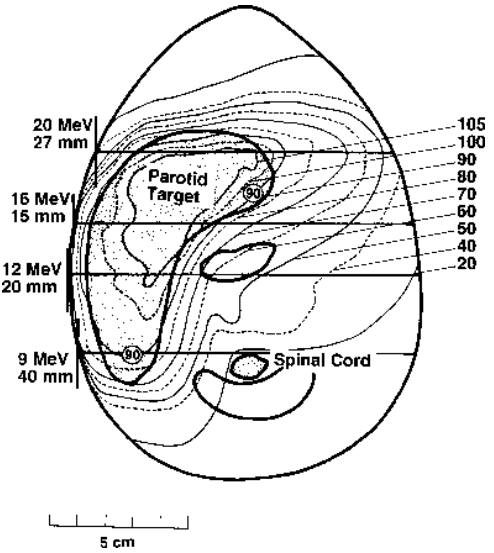

Figure 11. Dose distribution in a transverse plane through the parotid gland for a segmented-field ECT plan. The goal was coverage of the PTV by the 90% isodose contour while giving minimal dose to the spinal cord. [Reprinted from *Radiotherapy & Oncology*, vol 48, E. E. Klein, "Modulated electron beams using multi-segmented multileaf collimation," pp. 307–311. © 1998, with permission from Elsevier.]

Quality Assurance

The issue of quality assurance for segmented-field ECT has not specifically been reported. However, it should be possible to verify delivery by using film to measure the dose in three orthogonal planes in a cubical solid-water phantom, two orthogonal planes containing the beam's central axis, and one perpendicular to the central axis (depth ≈1 to 3 cm). The measured dose could be compared to that calculated in a cubical solid-water phantom, using the patient-specific beams.

Clinical Utility

Segmented-field ECT should be useful primarily in sites for which bolus ECT is useful (i.e., postmastectomy chest wall, parotid gland, and other head and neck sites that could benefit from ECT) to spare critical structures.

The major advantage of segmented-field ECT is that the dose fall-off beyond the 90% isodose surface distally is sharper than that with a bolus ECT treatment, as illustrated in figure 9. This is because bolus ECT requires that the maximum energy be used throughout the lateral extension of the field, and the $R_{90\text{-}10}$ is less for the lower energy electron beams that can be used for segmented-field ECT.

One disadvantage of segmented-field ECT results from the abutted fields not having matched penumbras, leading to dose inhomogeneity (hot and cold spots) in the abutment regions. This is evident in figure 9b, which shows hot spots of approximately 110% created just inside the edge of the higher energy beam. Varying the beam intensity near the beam edges to improve the matching of the penumbra could reduce or eliminate the dose inhomogeneity. Another disadvantage of segmented-field ECT is that the ability to conform the 90% dose surface might depend on the coarse energy resolution of existing radiotherapy accelerators; for example, the racetrack microtron has a rather coarse energy spacing of 5 MeV; the Varian Clinac 2100, an energy spacing of 3 to 4 MeV. Bolus, on the other hand, can be fabricated with a thickness accuracy of approximately 1 mm, corresponding to an energy spacing of 0.2 MeV. A final disadvantage arises if there are too many segmented fields; this leads to increased treatment time (or monitor units), which results in excess bremsstrahlung dose to the patient.

Intensity-Modulated Electron Therapy

In contrast to bolus ECT and segmented-field ECT, IMET is defined as the utilization of multiple electron beams, each with its own energy and intensity pattern. IMET differs from bolus and segmented-field ECT in that IMET allows electrons of multiple energies at a single point within the beam. On the other hand, bolus ECT can more finely vary the beam energy, whereas IMET is limited to the available energies of the treatment machine. IMET has a lesser surface dose than bolus ECT does because no bolus is present.

IMET has garnered increasing interest in recent years, and significant progress has been made in researching IMET planning and delivery techniques (Hyödynmaa, Gustafsson, and Brahme 1996; Åsell et al. 1997; Ebert and Hoban 1997; Lee, Jiang, and Ma 2000; Lee et al. 2001; Ma et al. 2000b, 2003). Figure 12, an example by Åsell et al. (1997), illustrates how IMET might be used for chest wall irradiation. Multiple energy electron beams, ranging from 5 to 30 MeV, conform the dose distribution to the chest wall. However, this example also illustrates other key issues. Most significant, possible techniques for delivering intensity patterns with such sharp gradients are not apparent. This emphasizes the significance of having an integrated treatment planning and delivery system, which is the essence of the discussion about treatment and treatment planning below. Second, the 5 MeV energy spacing of the radiotherapy machine used in this study is likely too great and undoubtedly would often result in excessive lung irradiation; however, the closeness of energy spacing necessary for MET has not been studied. Third, the solution space may be so complex that it might be difficult to define cost functions that provide highly practical solutions and avoid needless irradiation of normal tissues to doses below tissue tolerances.

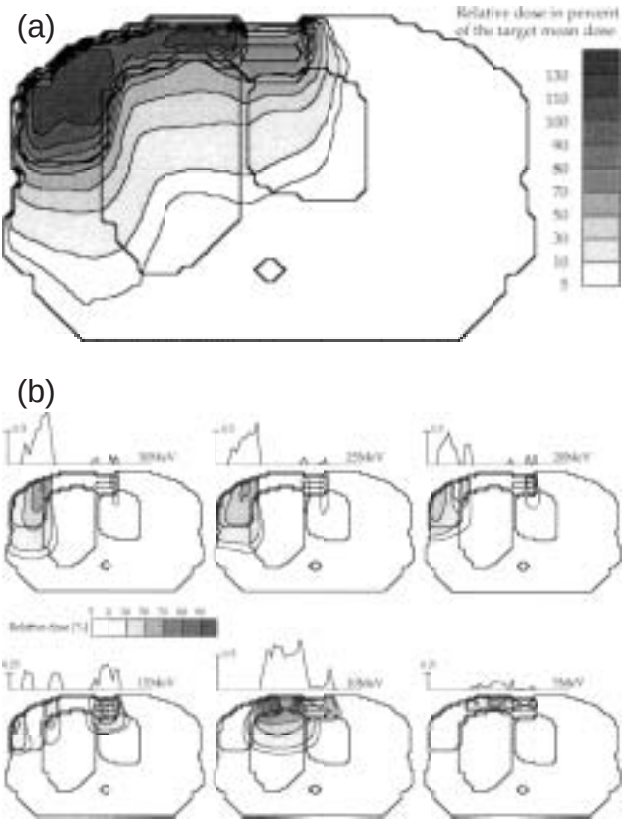

Figure 12. The potential of IMET is demonstrated by planning treatment of a chest wall phantom using a single beam portal in the anteroposterior (AP) direction. (a) The dose distribution resulting from six electron energies being used simultaneously is shown in a transverse plane. (b) The beam intensity versus position plot and the resulting dose distribution are plotted for each of the six electron beams, having energies ranging from 5 MeV to 30 MeV in 5 MeV steps. [Reprinted from *Physics in Medicine and Biology*, vol 42, M. Åsell, S. Hyödynmaa, A. Gustafsson, and A. Brahme, "Optimization of 3D conformal electron beam therapy in inhomogeneous media by concomitant fluence and energy modulation," pp. 2083–2100. © 1997, with permission from IOP Publishing.]

Treatment Planning—Optimization

Treatment planning for IMET differs from that for bolus ECT and segmented-field ECT in that it requires an inverse planning approach. Many inverse planning algorithms have been developed to optimize intensity-modulated radiation therapy (IMRT) using either photon beams or electron beams (Brahme 1988; Webb 1989; Holmes and Mackie 1994; Ebert and Hoban 1997; Jiang et al. 2000; Jiang, Pawlicki,

and Ma 2000; Ma et al. 2000b; Lee et al. 2001). IMRT planning is usually done by dividing a radiation field into small spatial elements, or beamlets, and determining the dose contribution from each beamlet as the first step in planning (ignoring leaf scatter and leakage). Optimizing the total dose distribution allows the weights or intensities for each beamlet to be obtained, and the resulting two-dimensional (2-D) intensity maps can be converted into an MLC leaf sequence for delivery. The optimization assumes that the dose computed on a beamlet-by-beamlet basis is the same as the dose delivered via the actual leaf sequence. In these instances, an additional adjustment must be applied to leaf sequences or simply during dose reconstruction so that planners can evaluate the true dose rather than an ideal dose.

Lee et al. (2001) proposed a solution to account for differences between the planned and actual MLC leaf sequence and differences in the dose between the planning and delivery stages; that solution is to perform a second optimization after a leaf sequence is determined. Considering a step-and-shoot leaf sequence algorithm, the leaf positions for each "shoot" segment define one or more small fields (segmented fields). Monte Carlo simulations of these MLC fields will be performed, which will be taken as a new set of "beamlets" in the second optimization. The second optimization will be fast because there are fewer segmented fields than initial beamlets, and thus it searches in a smaller solution space. In general, the outcome will not appear as optimal as that of the first optimization; however, the first optimization plan is nonrealistic without the leaf scatter and leakage effect. The idea behind the second optimization is that the leaf scatter and leakage effect can be minimized by reducing or increasing the weights of some segmented fields. This was demonstrated using a simple 2-D plan (Lee et al. 2001), as shown in figure 13. The target was chosen to be concave, with a critical structure placed within the concavity. A small region around the target was chosen to represent the normal tissue. The lateral extent of the target was approximately 20 cm. An array consisting of twenty 1-cm-wide beamlets was delivered into the phantom, covering the area from $x = -10$ to 10 cm. The resulting cumulative DVH is shown in figure 13. Idealized beamlets are optimized to give a dose distribution that agrees very well with the prescription, shown in figure 13 as a solid line. However, actual delivery of this plan adds the effect of the MLC leakage and scatter. The resulting DVH is right shifted and also has a change in the slope, suggesting poorer target coverage than was predicted by the idealized plan. However, once segment weights are re-optimized, the target coverage becomes very similar to that of the ideal beamlets, despite the non-idealities of the real collimator. The critical structure dose rises slightly with the addition of the leaves, owing to the leakage, but the final optimization reduces this effect somewhat. Figure 14 shows the intensity maps for different electron energies before and after the second optimization.

An alternative method to beamlet-based plan optimization is aperture-based plan optimization; for more information, the reader is referred to Jiang et al. (2000); Jiang, Pawlicki, and Ma (2000); and Deng, Lee, and Ma (2002).

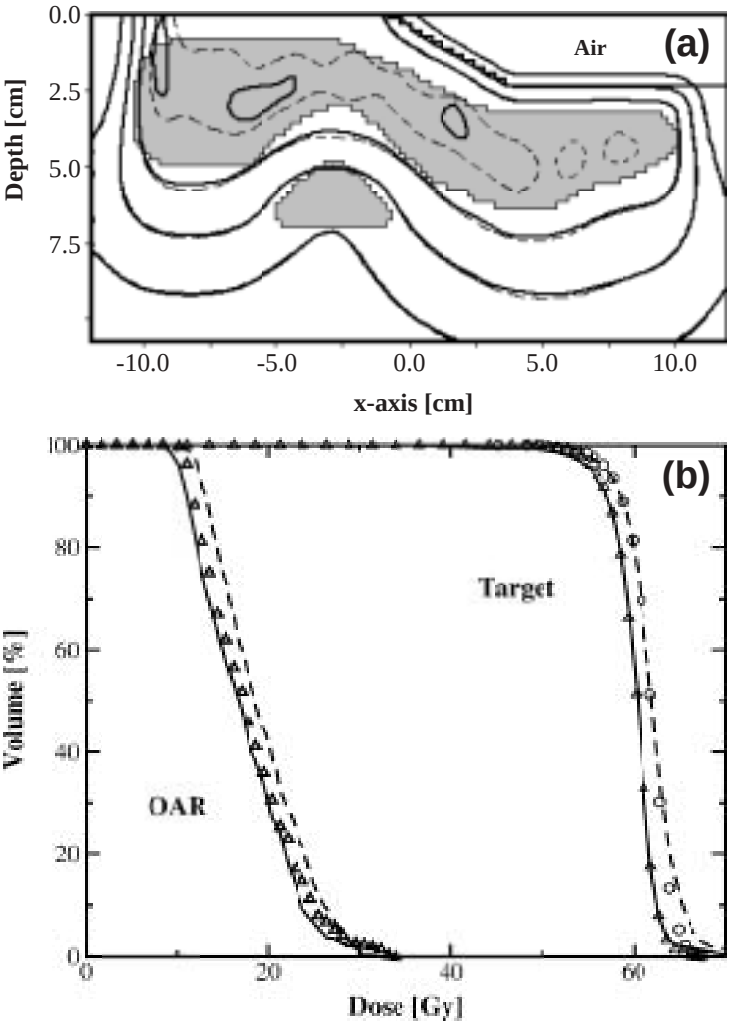

Figure 13. (a) Isodose plots for a 2-D homogeneous phantom. Shown are the simulated deliveries of plans generated accounting for leaf effects (solid) and ignoring leaf effects (dashed). Lines represent absolute dose: starting at the target moving outwards, 62.5, 50, 30, and 10 Gy. (b) DVHs for target and organ at risk (OAR): first optimization (solid), delivery of this plan with leaves in place without second optimization (dashed), and after second optimization (triangles). Also shown is the delivered target DVH (circles) for a plan in which a second optimization occurred, but in which segments only included leaf scatter, and not bremsstrahlung. [Reprinted from *Physics in Medicine and Biology*, vol 46, M. C. Lee, J. Deng, J. Li, S. B. Jiang, and C.-M. Ma, "Monte Carlo based treatment planning for modulated electron beam radiation therapy," pp. 2177–2199.]

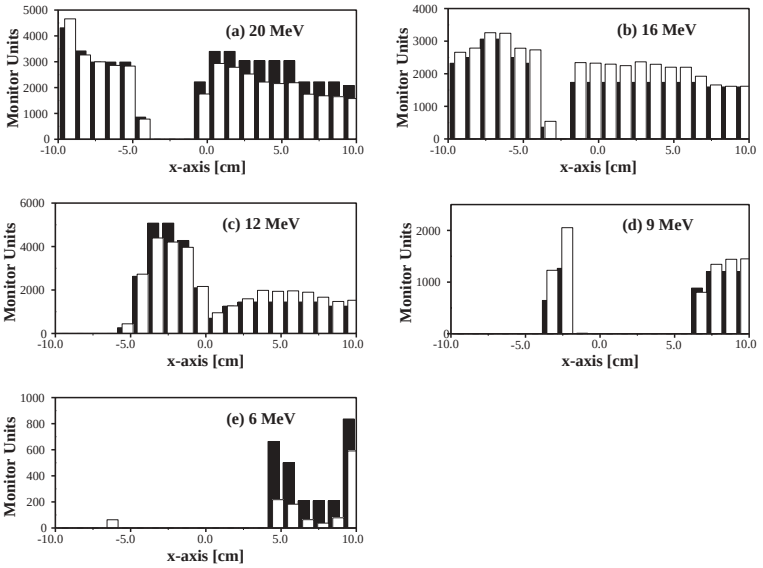

Figure 14. Intensity maps for different energies generated for the 2-D phantom plan of figure 13 by optimization of electron beamlets. Black bars = after first optimization; open bars = after second optimization. [Reprinted from *Physics in Medicine and Biology*, vol 46, M. C. Lee, J. Deng, J. Li, S. B. Jiang, and C.-M. Ma, "Monte Carlo based treatment planning for modulated electron beam radiation therapy," pp. 2177–2199.]

Treatment Planning—Dose Calculation

As emphasized above, the accuracy of dose calculation plays an important role in the treatment planning optimization process for intensity-modulated therapy because the beamlet dose distribution in the heterogeneous patient geometry must be accurate and the effect of MLC leaf leakage and scatter must be accounted for (Jeraj and Keall 1999; Ma et al. 1999b, 2000a; Pawlicki and Ma 2001; Siebers et al. 2002). This requirement is more stringent for electron beams than for photon beams owing to electron scattering in the treatment head, in the air between the treatment head and the patient, and inside the patient (Lee, Jiang, and Ma 2000; Ma et al. 2000b; Lee et al. 2001). Conventional pencil-beam dose algorithms appear insufficiently accurate for IMET owing to the inaccuracy for small fields, extended air gaps, and regions near material interfaces and inhomogeneities. Ma et al. (2000b) compared beamlet dose distributions computed using a 3-D pencil-beam algorithm, as implemented in the FOCUS treatment planning system (Computerized Medical Systems, St. Louis, MO), with those computed using a Monte Carlo algorithm. Figure 15 shows the dose distributions calculated using the Monte Carlo method (a, c) and the FOCUS 3-D

pencil-beam algorithm (b, d) for a 1×1 cm^2, 12 MeV beamlet incident on a patient phantom built from CT data. For beamlets with normal incidence and a 10 cm air gap (figures 15a and 15b), the difference in the dose distributions in the heart was evident: the Monte Carlo calculated isodose lines varied with the heart contour, whereas the pencil-beam calculated isodose lines remained symmetrical despite the change in material densities. Figures 15c and 15d show the beamlet distributions for oblique incidence. The axis of the beamlet was intentionally placed to go through soft tissues and bones. The pencil-beam isodose lines seemed to stretch according to the beam axis path-length and showed no signs of electron build down near the lung.

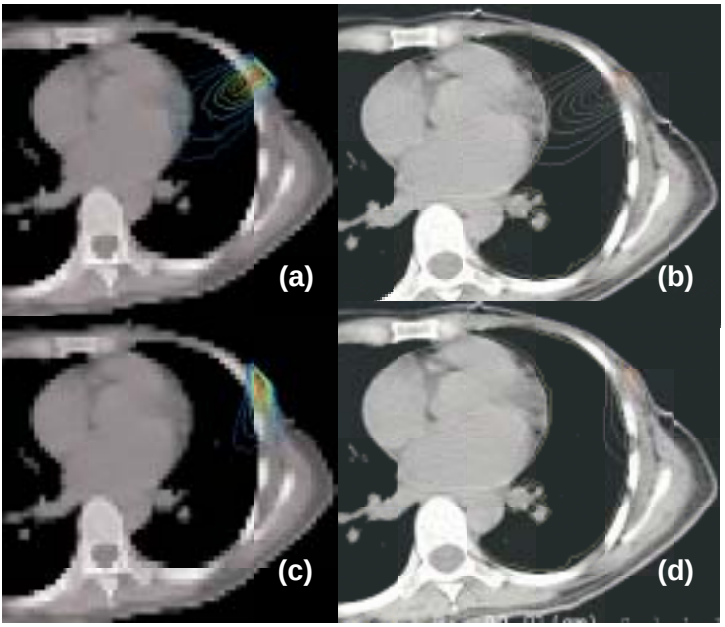

Figure 15. Comparison of dose distributions calculated using the Monte Carlo method (a,c) and the FOCUS 3-D pencil-beam algorithm (b,d) for a 1×1 cm^2, 12 MeV beamlet. The beamlet size is defined at 100 cm SSD. Two geometries are compared, normal incidence with 10 cm air gap (a,b) and oblique incidence (c,d). The isodose lines shown are 10, 20, 30, 40, 50, 60, 70, 80, and 90% of the maximum dose. [Reprinted from *Physics in Medicine and Biology*, vol 45, C.-M. Ma, T. Pawlicki, M. C. Lee, S. B. Jiang, J. S. Li, J. Deng, B. Yi, E. Mok, and A. L. Boyer, "Energy- and intensity-modulated electron beams for radiotherapy," pp. 2293–2311. © 2000, with permission from IOP Publishing.]

The results of Ma et al. (2000b) indicated that accurate dose calculation algorithms, such as Monte Carlo simulations (Mackie et al. 1994; Ma and Jiang 1999), are needed to compute electron beamlet distributions for the inverse planning process. Accurate dose calculation is also needed by IMET to account for the effect of bremsstrahlung leakage through the MLC leaves, electron scattering off the MLC leaf

edges, and electron scattering in the air and inside the treatment head. Lee, Jiang, and Ma (2000) investigated the accuracy of Monte Carlo simulations and found good agreement with film measurement. Also, the Monte Carlo method has been found to be a useful tool for electron collimator design because of its ability to simulate electron transport accurately in complex geometry (Ma et al. 2000b).

Treatment Delivery

Different techniques have been explored for IMET beam delivery. Utilization of a scanned electron beam for intensity modulation has been demonstrated (Lief, Larsson, and Humm 1996; Karlsson, Karlsson, and Zackrisson 1998); however, these applications were for lower gradients in the incident fluence than the gradient likely needed for IMET. At lower beam energies, the dose kernel width can become excessively large, making a scanned electron beam less attractive for IMET. Also, scanned beams are not available on commonly used clinical accelerators.

The most practical method for MET beam delivery might be the use of MLCs. X-ray MLCs are available but generally impractical for electron beams because of the large air gap between them and the patient; this results in inadequate lateral resolution of the pencil beams due to electron scatter in the air and scattering foil system (Brahme 1987; Zackrisson and Karlsson 1996; Janssen et al. 1997; Karlsson, Karlsson, and Ma 1999; Lee, Jiang, and Ma 2000; Ma et al. 2000b; McNeeley et al. 2001). One of the advantages of using an x-ray MLC is that x-ray and electron beams may be easily combined in the same plan. An essential requirement for matching an x-ray beam and an electron beam at different depths is that both beams share the same virtual source position. To accomplish this, several modifications to the design of a Varian Clinac 2300CD accelerator have been proposed (Karlsson, Karlsson, and Ma 1999). One proposed modification was to relocate the treatment head's dual scattering foil system to place the electron virtual source near that of the x-ray beam. Another was to replace the air in the treatment head with helium, which could significantly reduce the effect of electron scattering in the air on the beam penumbra. However, both of these proposed modifications require major changes to the existing treatment head design. Also, the beam properties deteriorate significantly for energies below 6 MeV, even for a helium-filled treatment head (Lee. Jiang, and Ma 2000).

Another alternative is to fabricate multiple electron cutouts. Although multiple electron cutouts are easy to fabricate and implement for small-scale clinical applications, their application to IMET would be too labor intensive and time consuming. To solve this problem, Ma et al. (2000b) investigated an alternative solution, a thin-leaf MLC at the electron cutout level to reduce the air scattering effect (figure 16a). The prototype eMLC consisted of 30 steel leaf pairs. Each leaf was 0.476 cm wide (0.5 cm projected to isocenter), 20 cm long, and 2.54 cm thick, with straight edges and ends. The leaves were mounted on a steel frame attached to the bottom scraper of a 25×25 cm^2 electron applicator on a Varian Clinac 2100C. The leaves slide in the steel frame, and the leaf positions are easily set using a precut cardboard for a beam segment. The

largest radiation field available using the electron MLC was 15.7×15.7 cm^2, projected at 100 cm SSD (source-to-surface distance). A different eMLC design has been reported by McNeeley et al. (2001). Hogstrom and colleagues (Antolak, Boyd, and Hogstrom 2002; Boyd, Antolak, and Hogstrom 2002) designed a similar device for a Siemens PRIMUS accelerator (figure 16b); however, it was designed to be an applicator replacement and to be retractable. Their prototype utilized 3.0 cm thick brass leaves that had a 1 cm width projected to isocenter. The leaves could form a field up to 21×20 cm^2 and matched those of the PRIMUS x-ray MLC. Also, their design had diverging-leaf cross sections and rounded ends so that the electron scatter was minimal and penumbra independent of collimator position.

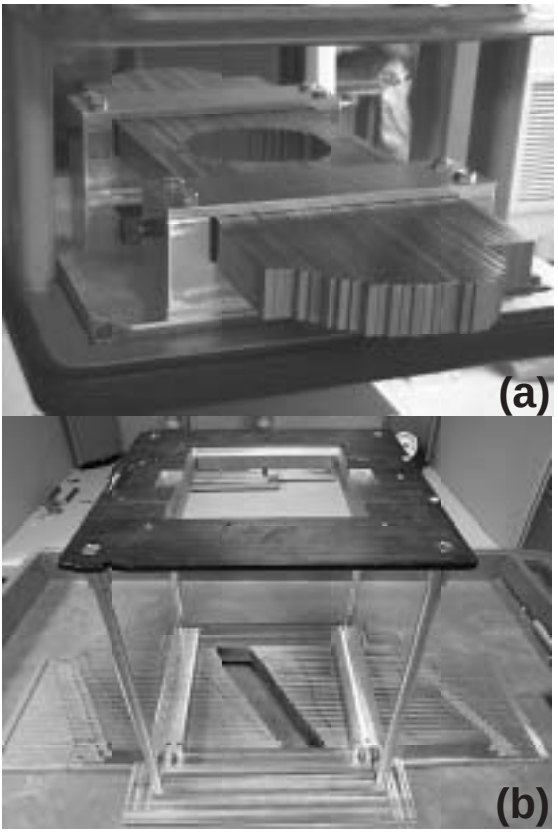

Figure 16. (a) Stanford prototype eMLC mounted in a 25×25 cm^2 applicator of a Varian 2100C accelerator. [(a) Reprinted from *Physics in Medicine and Biology*, vol 45, C.-M. Ma, T. Pawlicki, M. C. Lee, S. B. Jiang, J. S. Li, J. Deng, B. Yi, E. Mok, and A. L. Boyer, "Energy- and intensity-modulated electron beams for radiotherapy," pp. 2293–2311. © 2000, with permission from IOP Publishing.] (b) M. D. Anderson prototype eMLC designed for a Siemens Primus accelerator (Antolak, Boyd, and Hogstrom 2002).

Because of its thinner leaves and shorter distance to the patient surface, an eMLC can provide better dosimetric properties for small-field electron beams than an x-ray MLC can. Lee, Jiang, and Ma (2000) reported Monte Carlo and experimental investigations of multileaf collimated electron beams for IMET. They studied two proposed methods of electron-beam collimation: the use of existing x-ray MLC in a helium atmosphere to reduce in-air electron scatter, and an MLC specifically designed for electron-beam collimation. They concluded that an eMLC will have dosimetric characteristics similar to those of an x-ray MLC with focused leaf ends, but without the need to replace the air in the accelerator head with helium. The major disadvantage of the eMLC is its inablility to attenuate the contaminant bremsstrahlung dose in the electron beams. This effect is illustrated in figure 17, which shows Monte Carlo calculated dose distributions for a single 4×4 cm^2 electron field and a multiple abutting field of the same size formed by four 1×4 cm^2 electron fields. For a 20 MeV electron beam, the dose at the phantom surface for the abutting field shows about 4% fluctuation compared with that for a single electron field. This may result from the effect of leaf shape and extended source. The dose outside the field for the abutting field is about three times higher than it is for the single field; this effect is mainly caused by the leaf x-ray leakage. This is due to the longer beam-on time to deliver the four 1×4 cm^2 fields and electrons scattering off the leaf ends. This increased leakage is comparable to that for photon IMRT, where the beam-on time is generally 2.5 to 3.5 times longer than it is with a conventional photon treatment. The dose at a 3 cm depth shows little difference between the abutting field and the single field, except for the dose near the field edges and outside the field. For a 6 MeV electron beam, the dose at the phantom surface for the abutting field is almost the same as that for the single field (not shown). The effect of leaf leakage is very small for a 6 MeV beam, and the dose immediately outside the field is thought to be caused mainly by the effect of electron scattering in the air. It seems that field abutting with 1 cm beamlets collimated by an electron MLC can provide adequate beam characteristics for IMET for the beam energies investigated. However, the dose outside the field needs to be minimized through beam energy and leaf-sequence optimization.

Clinical Utility

IMET should have the same clinical utility as the previously discussed MET techniques have. One potential untested application of IMET not previously discussed is treatment of intact breast. Figure 18 shows isodose plots, comparing 6 MV x-rays with IMET with 6, 9, 12, 16, and 20 MeV electrons (Ma et al. 1999a) in a left breast with a large target volume. Also, the x-ray plan included a 1.5 cm margin to account for breathing motion, whereas the IMET plan did not require this extra margin. The DVH curves shown in figure 18 demonstrate that with more energies to optimize, the lung dose can be significantly improved. The intermediate doses (25 to 50 Gy) were completely removed, and the lung volume that received a low dose (less than 3 Gy) was almost the same as that for the tangential photon beams, indicating that the bremsstrahlung effect was not significant with eMLC modulation. The improvement

to the heart dose is equally significant with IMET. Further improvement in the target dose uniformity may be achieved through beam orientation optimization, i.e., by using more beam angles in the IMET optimization.

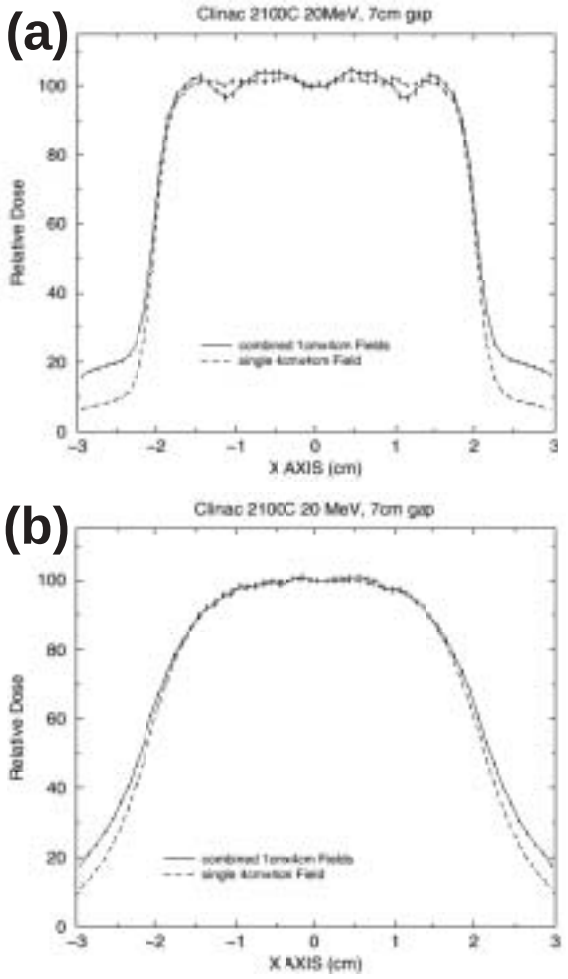

Figure 17. Demonstration of impact of x-ray leakage when using an eMLC for IMET. Monte Carlo calculated off-axis dose profiles in a water phantom for a 20 MeV electron beam collimated by an electron MLC of 1.5 cm thick tungsten leaves for a single 4×4 cm^2 electron field and for a 4×4 cm^2 field formed by four 1×4 cm^2 electron fields at depths of 0.5 cm (a) and 3 cm (b). [Reprinted from *Physics in Medicine and Biol*ogy, vol 45, C.-M. Ma, T. Pawlicki, M. C. Lee, S. B. Jiang, J. S. Li, J. Deng, B. Yi, E. Mok, and A. L. Boyer. "Energy- and intensity-modulated electron beams for radiotherapy," pp. 2293–2311. © 2000, with permission from IOP Publishing.]

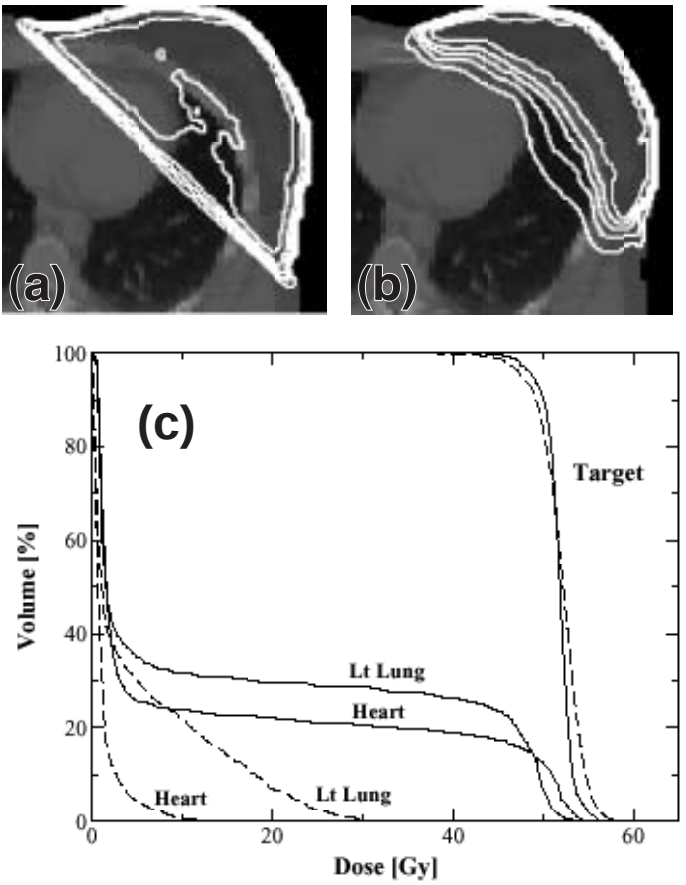

Figure 18. Comparison of dose distributions resulting from standard tangential 6 MV x-ray beams (a) with that from IMET (b) for intact breast irradiation. Isodose curves at 10, 20, 30, 40, and 50 Gy are plotted. (c) DVH plots for the target, heart, and left lung resulting from tangential 6 MV x-ray beams (solid lines) and from IMET (dashed lines) are compared (Ma et al. 1999).

Figure 19 shows the patient anatomy and isodose contours for intact breast irradiation; treatment was planned using intensity-modulated tangential beams, four-field IMXT, and eight-field IMET (Ma et al. 2003). The corresponding DVHs for the target, lung, and heart are shown in figure 20. This patient had a relatively thin breast and a flat chest-wall and therefore represented a more favorable case for tangential beams because less lung and heart would be exposed to the x-ray beams. However, conventional tangents usually result in higher doses in the thinnest regions of the breast (superior and inferior borders near the apex). These region-specific hot spots are most likely to manifest as clinical side effects, such as edema. Greater flexibility in intensity

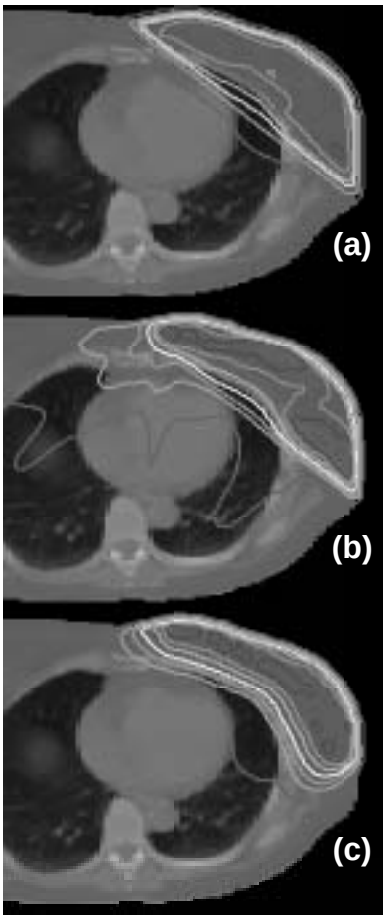

Figure 19. Isodose plots planned using two intensity-modulated tangential beams (a), four-field IMXT (b) and 8-field IMET (c) for a patient with breast cancer. The dose distributions are normalized to deliver 50 Gy to the 95% target volume. The 55, 52.5, 50, 45, 40, 25, 15, and 5 Gy isodose lines are shown. [Reprinted from *Physics in Medicine and Biology*, vol xx (submitted), C.-M. Ma, M. Ding, J. S. Li, M. C. Lee, T. Pawlicki, and J. Deng. (2003), "A comparative dosimetric study on tangential photon beams, IMRT and MERT for breast cancer treatment." © 2003, with permission from IOP Publishing.]

modulation allowed IMXT tangents to correct for this, though hotspots in entrance tissue may still occur especially in patients with large breasts. The dose heterogeneity in the target is greater with IMET (about 10%) than with IMXT tangents (about 5%), but it is better than with the four-field IMXT plan (about 15%). The lung and heart doses are much less than 20 Gy in the IMET plan. Unlike the x-ray plans, dose hotspots in the IMET plan were found to be more widely dispersed throughout the target region, not localized in specific geometric features. The multiple field IMXT technique was

apparently inferior for breast treatment, with significant lung and heart volumes receiving low and medium doses (cf., figure 20a). It is also evident from the doses in healthy tissues (which represent everything inside the patient—external contour less the target volume) that multiple-field IMXT was inferior to intensity-modulated tangents and IMET. The volume of healthy tissues that received a 5 Gy dose was greater than 5000 cm^3 with four-field IMXT compared with less than 2000 cm^3 with intensity-modulated tangents and IMET (figure 20b). Because radiation-induced fatal risk is proportional to the integral dose (total energy deposited in the body), it is likely that IMET can be more beneficial than conventional tangents or IMXT in terms of late effects; however, more detailed studies are needed to make a general conclusion.

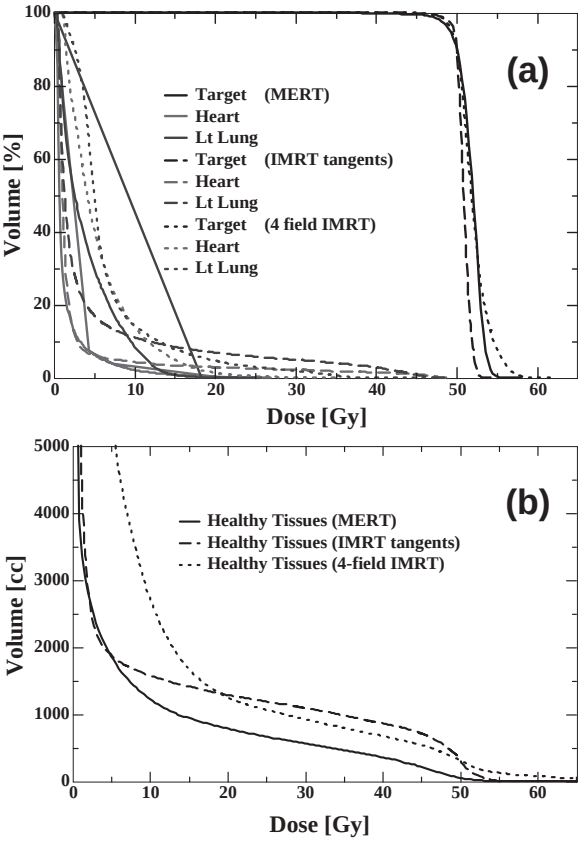

Figure 20. Dose-volume histograms for the target, lung, and heart (a) and healthy tissues, defined as all non-target volumes in the body (b), for the three intensity-modulated plans in figure 19. [Reprinted from *Physics in Medicine and Biology*, vol xx (submitted), C.-M. Ma, M. Ding, J. S. Li, M. C. Lee, T. Pawlicki, and J. Deng. (2003), "A comparative dosimetric study on tangential photon beams, IMRT and MERT for breast cancer treatment."]

Modulated Electron Arc Therapy

Modulated electron arc therapy (MEAT) is defined as the utilization of multiple arced beams of differing energies, with beam intensity varying with position along the arc and along the accelerator's isocentric axis. To achieve a uniform maximum dose (D_{100}) throughout the field, the electron beam fluence incident on the patient's surface has been varied by altering the width of the electron collimator (Hogstrom and Leavitt 1987). Present treatments utilize a fixed applicator, and the secondary collimator width is varied along the cephalo-caudal direction to account for variations in the patient's mean radius of curvature (i.e., distance from isocenter to patient surface along radial line) between transverse planes. Typically, the radius of curvature is less superiorly (lower neck) than inferiorly (lower chest). However, the radius of curvature within a single transverse plane can vary considerably, requiring that the secondary collimator width also vary with position along the arc. In other words, the secondary collimator width W should vary with both position along the cephalo-caudal dimension (Y) and position along the angle of arc (θ). Leavitt et al. (1989b) have demonstrated that this can be achieved by replacing the fixed secondary collimator with an eMLC whose shape varies with arc position [i.e., width $W = W(Y,\theta)$].

Electron arc therapy is used almost exclusively for treating postmastectomy, chest-wall cancer, where the PTV depth is the chest-wall thickness along rays emanating from isocenter. This is exemplified in figure 21, a typical patient treatment plan, in which one beam energy treats the internal mammary chain and another treats the chest wall, whose thickness is reasonably constant. However, the chest wall thickness might not always be constant. In some instances the postmastectomy chest wall has a highly variable thickness owing to excision of a significant portion of tissue. In such cases, custom bolus can be used to restore a constant thickness (Tobler and Leavitt 1996), much as that designed for fixed-beam bolus ECT and discussed above. Development of tools similar to those used for designing and constructing bolus for bolus ECT would enhance this process. An alternative technique would be to partition the beam energy in Y as well as in θ [i.e., $E = E(Y,\theta)$], using techniques similar to those used for fixed-beam MET above, namely, segmented-field ECT or IMET. Because these techniques are just beginning to be investigated, we will discuss a general vision and needs for their future use.

Treatment Planning

The area to be treated using arc therapy can be viewed in the same sense as the area to be treated with segmented-field ECT. The electron beam energies can be partitioned using a beam's eye view (i.e., viewing the patient anatomy from the virtual source of the electron beam). There is not a single virtual point source in MEAT, and although this does not create a problem, it does require a different way of thinking of the beam's eye view. In the plane of rotation, the mean directions of the electrons are focused toward isocenter. In a plane containing the central axis of the beam and the isocentric

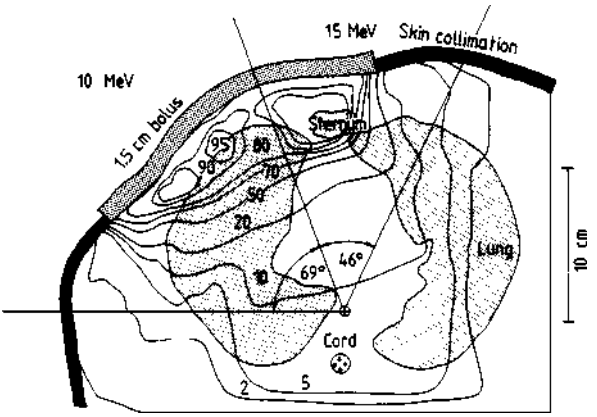

Figure 21. Typical arc electron treatment plan for a postmastectomy chest wall. Note that this patient required bolus to attain an adequate surface dose and to conform the 90% dose contour to the lung-chest wall interface. The plan required two beam energies, 15 MeV for the IMC and 10 MeV for the chest wall. Variation in chest-wall thickness in 3-D could require additional arced beams of different energies, similar to segmented-field ECT. Variation in the isocenter-to-patient-surface distance in 3-D could require methods for optimizing dose homogeneity, such as by varying secondary collimator width with angle of arc. [Reprinted from *Physics in Medicine and Biology*, vol 34, K. R. Hogstrom, R. G. Kurup, A. S. Shiu, and G. Starkschall, "A two-dimensional pencil-beam algorithm for calculation of arc electron dose distributions," pp. 315–341. © 1989, with permission from IOP Publishing.]

axis of the gantry, the virtual point source is the same as for a fixed beams (cf., figure 22; Hogstrom and Leavitt 1987). If a regular array of points is defined on the surface of a cylinder, the mean direction of electrons passing in the vicinity of each point is well defined and can be used to generate a PTV depth map. The beam energy can also be partitioned [$E = E(Y,\theta)$] so that the 90% dose surface encompasses the PTV, while conforming as closely as possible to its distal surface. Experience from 2-D–arc therapy planning shows that the boundary of the higher energy beams must extend adequately to account for electron penumbra. This can be appreciated from the two-energy plan previously shown for a single transverse plane (cf., figure 21).

Once the treatment is segmented for beam energy, $E(Y,\theta)$, it can be partitioned for collimator width, $W(Y,\theta)$, which controls dose uniformity. This can be calculated using the simple formula provided by Hogstrom and Leavitt (1987) and Leavitt et al. (1989b).

Because of the large air gap between the secondary collimator and the patient, the dose distribution at the end of an arc is large and its shape results largely from beam geometry (i.e., the collimator width). This provides broad matched penumbras, well suited for abutting arced beams of differing energy (Khan et al. 1991). A broad penumbra at the edges of the PTV can be made sharp by arcing 15° beyond the azimuthal extent of the PTV using skin collimation to restore the penumbra.

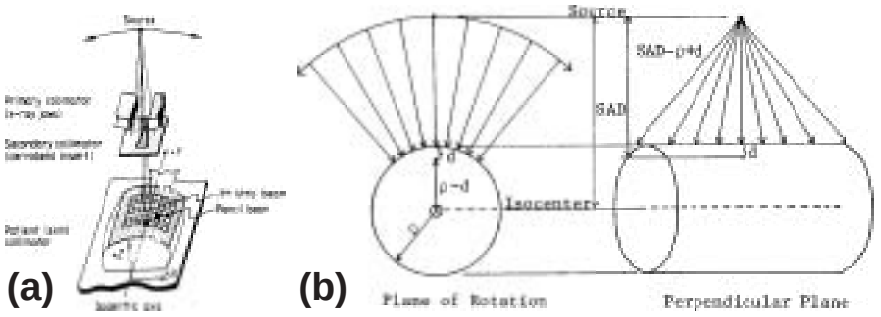

Figure 22. Geometry of arc therapy. (a) Illustration of the relationship between the x-ray collimator, secondary collimator (used to control dose homogeneity), and skin collimation on the patient. Note that the patient irradiated area can be partitioned into pixels for the purposes of treatment planning and dose calculation. [(a) Reprinted from *Physics in Medicine and Biology*, vol 34, K. R. Hogstrom, R. G. Kurup, A. S. Shiu, and G. Starkschall, "A two-dimensional pencil-beam algorithm for calculation of arc electron dose distributions," pp. 315–341. © 1989, with permission from IOP Publishing.] (b) Mean directions of electrons in plane of rotation are focused toward isocenter, and mean directions of electrons in plane perpendicular to isocenter show electrons emanating from a point source. [Reprinted from K. R. Hogstrom and D. D. Leavitt. "Dosimetry of Arc Electron Therapy" in *Radiation Oncology Physics–1986*, J. G. Kereiakes, H. R. Elson, and C. G. Born (eds.), pp. 265–295. © 1987, with permission from American Institute of Physics.]

Interestingly, for each beam, $E(Y,\theta)$ and $W(Y,\theta)$ are mostly independent of each other. Once specified, the dose distribution is calculated in 3-D. A first approximation to monitor units can be determined for each arc by prescribing to 90% of the maximum dose. Monitor units could be optimized to give the most uniform dose in the PTV while still conforming the 90% dose surface to the PTV. An alternative approach might be one similar to IMET, where beamlets are specified by beam energy (E), arc angle (θ), eMLC leaf index (Y), and eMLC strip width (W).

Presently, treatment planning systems lack adequate capability for 3-D dose calculations for arc electron therapy. Dose calculation could likely utilize analytical or Monte Carlo methods. The algorithm could be configured to simulate an arced beam as (1) a collection of fixed beam dose calculations or (2) a two-step calculation. The latter transports electrons from the arced beam to the patient surface, where the skin surface is partitioned into pencil beams, and for each pencil beam the dose to the patient is calculated. This was the approach of Hogstrom et al. (1989) for multiplane, 2-D dose calculations, which could easily be extended to 3-D. However, with the ever-increasing speed of computers, it now seems more practical to simulate arc-beam dose distribution by summing fixed-beam dose calculations. Additionally, dose algorithms for arc electron therapy require the ability to model skin collimation and to accurately calculate x-ray dose.

In summary, treatment planning tools and dose-calculation tools must be developed and implemented into 3-D treatment planning systems before MEAT can be practical.

Treatment Delivery

Treatment for this therapy will consist of an arced beam for each of the beam energies comprising a patient's treatment plan. Each arc will be specified by a range of arc rotation (θ_{start},θ_{stop}), a number of monitor units to be delivered, and a variable collimator width $W(Y,\theta)$. Leavitt et al. (1989b) demonstrated that the latter could be accomplished by replacing the fixed, secondary collimator with a computer-controlled, dynamic MLC. Their prototype eMLC, pictured in figure 23, had a 4 cm leaf width projected to isocenter.

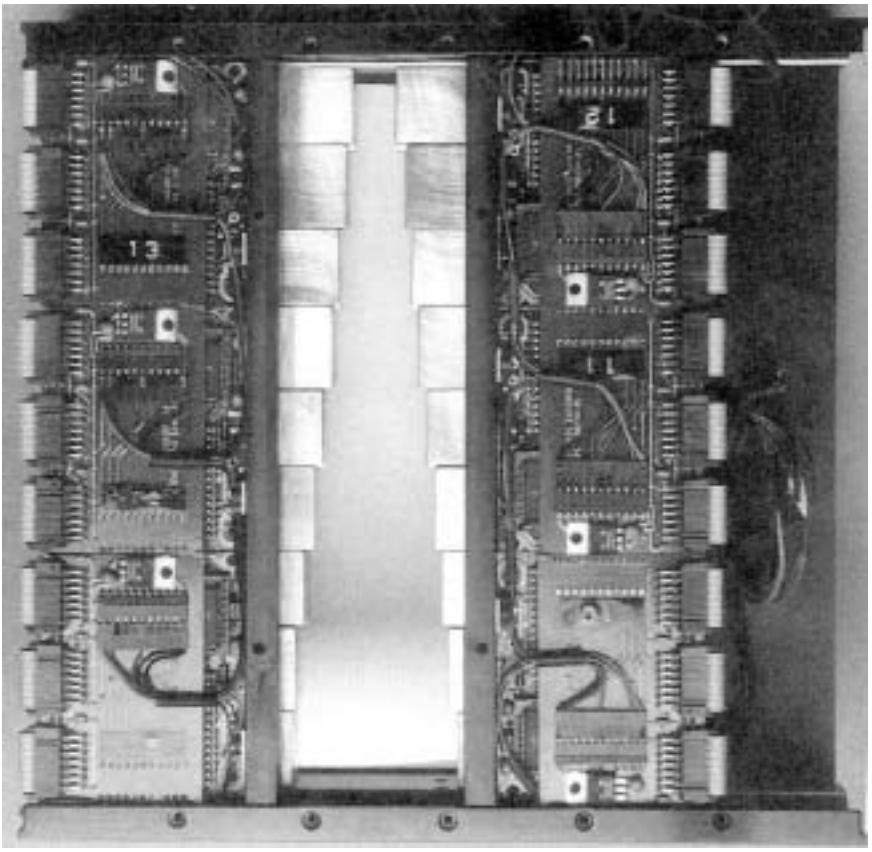

Figure 23. Beam's eye view of prototype eMLC for electron arc therapy. The leaf resolution (approximately 4 cm projected to isocenter) is coarse but could easily be improved. [Reprinted from *International Journal of Radiation Oncology Biology Physics*, vol 17, D. D. Leavitt, J. R. Stewart, J. H. Moeller, W. L. Lee, and G. A. Takach, Jr., "Electron arc therapy: Design, implementation and evaluation of a dynamic multi-vane collimator system." pp. 1089–1094. © 1989, with permission from Elsevier.]

Quality Assurance

Beam uniformity can be verified by *in vivo* dosimety on the chest wall surface using thermoluminescent dosimetry (TLD) or another appropriate dosimeter. Presently, methods have not been developed to verify the penetration of electron dose. However, a method similar to that standardly used for IMXT can be envisioned. Film could be used to measure the dose distribution in multiple transverse planes in a 30 cm diameter, cylindrical, solid-water phantom. The treatment planning system would calculate the dose in this phantom using patient-specific beam parameters, and those results would be compared to measurement for verification.

Clinical Utility

The primary utility of MEAT will likely be postmastectomy chest wall therapy. The utility of intensity modulation to achieve dose uniformity was demonstrated by Leavitt et al. (1989a, c.f., figure 24). The patient's radius of curvature in the plane of rotation varied from approximately 12 cm to 19 cm, resulting in significant dose non-uniformity (approximately 70% to 110%) using a fixed collimator width. Allowing the field width to change 10 times over the approximately 190° arc improved the dose uniformity (to approximately 90% to 105%). This example utilized a single beam energy, although typically two energies are required, one for the chest wall and one for the internal mammary chain.

The radial depth dose in arc electron therapy shows considerably less surface dose (60% to 70%) than do fixed electron beams (cf., figure 25a). Leavitt, Stewart, and Earley (1990) have demonstrated the benefit of the superposition of multiple electron energies across an arc segment to achieve increased surface dose and improved radial depth dose uniformity (cf., figure 25b). Consequently, the benefit of an IMET-like technique for MEAT might be beneficial.

Mixed-Beam Therapy

Mixed-beam therapy is defined as the combining of electron and photon beams for the purpose of achieving a more optimal patient dose distribution. Mixed-beam therapy includes both conventional and conformal therapy for the electron and photon beams.

The mixing of electron with x-ray therapy offers further benefits over either modality individually. Although the abutment of x-ray with electron fields offers significant treatment opportunities, mixed-beam therapy in the present context will be limited to the utilization of electron and x-ray beams to irradiate the same PTV. Historically, x-rays have been mixed with electrons to decrease surface dose, to increase therapeutic depth, and/or to increase dose homogeneity in the PTV (Fields and Hogstrom 1984). Such mixed-beam therapy has been utilized for irradiation of head and neck cancers and for irradiation of the IMC (Tapley 1976).

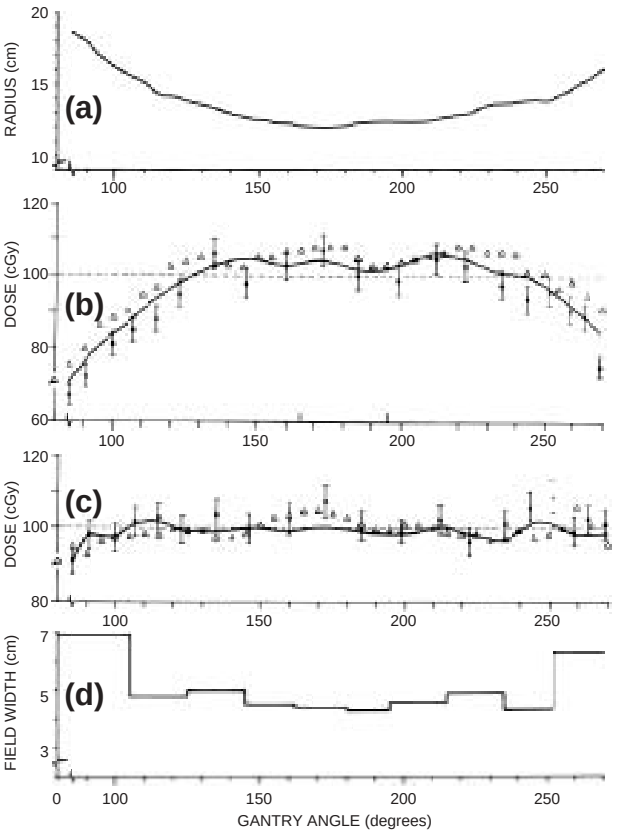

Figure 24. Utility of eMLC for bilateral arc therapy. (a) Radius of curvature versus arc position (gantry angle) varies significantly in superior transverse plane of patient. (b) Treatment with a constant-width secondary collimator produces significant dose inhomogeneity, as shown in plot of maximum depth dose versus arc position. (c) Treatment with a variable-width secondary collimator produces a uniform dose, as shown in the plot of maximum depth dose versus arc position. (d) Plot of secondary collimator width versus arc position required to achieve the dose in (c) above. [Reprinted from *International Journal of Radiation Oncology Biology Physics*, vol 16, D. D. Leavitt, J. R. Stewart, J. H. Moeller, and L. Earley, "Optimization of electron arc therapy doses by multi-vane collimator control," pp. 489–496. © 1989, with permission from Elsevier.]

IMXT and MET are at two ends of the treatment spectrum. Either can provide a conformal treatment to a superficial PTV, each having different strengths and weaknesses, as demonstrated above for irradiation of an intact breast. Using a similar technique, Li et al. (2000) found the mixed-beam IMRT to show improvement over the conventional tangential field technique, giving a reduced dose to the ipsilateral lung and heart.

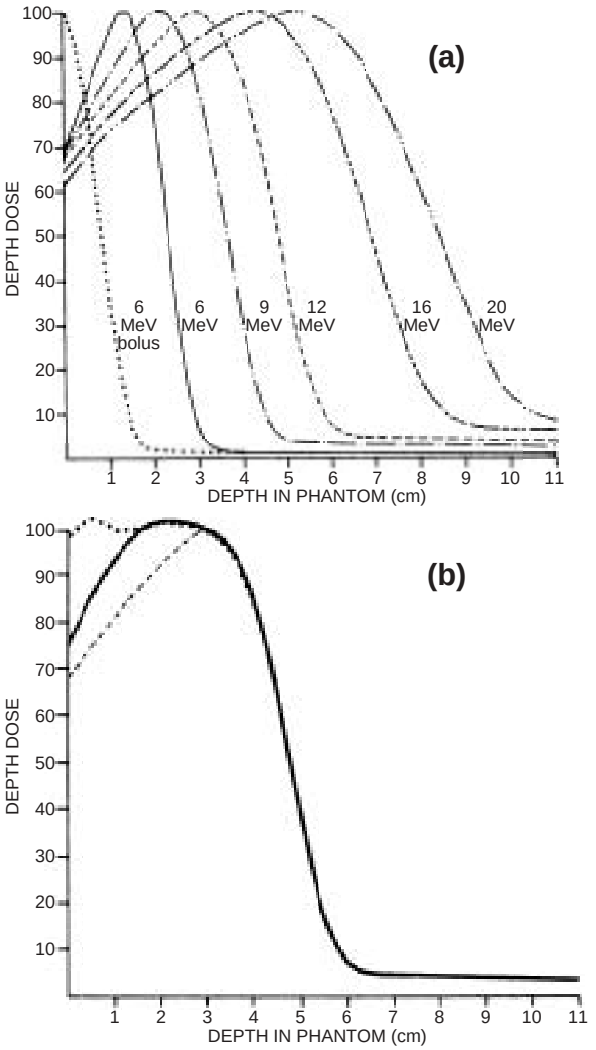

Figure 25. Utilization of energy modulation to achieve improved homogeneity of depth dose in MEAT. (a) Depth doses for an electron arc of 90° incident on a cylindrical phantom of 15 cm radius. Isocenter depth was set to 15 cm. Depth doses for 6, 9, 12, 16, and 20 MeV are shown, as well as the depth dose for a 6 MeV beam supplemented by 1.5 cm thick bolus. (b) Depth doses for a 12 MeV arced beam (dashed); addition of 6, 9, and 12 MeV arced beams (solid); and addition of 6, 9, 12 MeV, and "bolused" 6 MeV arced beams (dotted). [Reprinted from *International Journal of Radiation Oncology Biology Physics*, vol 19, D. D. Leavitt, J. R. Stewart, and L. Earley, "Improved dose homogeneity in electron arc therapy achieved by a multiple-energy technique," pp. 159–165.]

Svatos, Rosenman, and Verhey (2000) showed the potential of mixed-beam therapy for reduced integral dose for superficial tumors (0 to 4 cm depth). Medical physicists at M. D. Anderson have seen similar potential in comparing bolus ECT with IMXT plans for head and neck cancers. Therefore, the mixture of the two modalities can be expected to find a future role in patient care.

Conclusion

MET is a modality that offers improved electron therapy for patients, particularly those having disease near the surface and those having critical structures underlying the PTV. Methods for bolus ECT are well refined, and the clinical utility of this modality has been demonstrated for chest wall and head and neck cancer. This technology is not widely available because treatment planning manufacturers have not incorporated proven treatment planning methods into their treatment planning systems.

Segmented-field ECT provides an alternative to bolus ECT, and its utilization has also been demonstrated for the same sites; its main advantages are that it does not require fabrication of a bolus and that it has a sharper dose fall-off in depth from the PTV ($R_{90\text{-}10}$). This technology is not widely available, primarily owing to radiotherapy manufacturers not offering adequate MLCs and treatment head design.

IMET offers an inverse planning approach, which offers improved dose uniformity in the PTV. It is expected to provide an alternative to bolus ECT and segmented-field ECT in chest wall and head and neck treatments. Although more complicated than the previous two techniques, IMET also offers the potential for improved dose distributions and application in other major areas, e.g., intact breast.

These electron conformal therapy methods, with some modifications, can be applied to modulated arc electron therapy, which is most useful in the treatment of the postmastectomy chest wall. Finally, the ability to offer MET should allow its mixing with IMXT, providing treatment that is better than either modality alone, i.e., taking advantages of the strengths and weaknesses of each modality in a single treatment.

For these techniques to become available, research must continue to provide adequate tools for plan optimization, dose calculation, treatment delivery, and quality assurance and must demonstrate their clinical utility. Most important, unless the radiation oncology community can convince treatment planning system and radiotherapy accelerator manufacturers of its need, commercial availability and hence its widespread use will not be possible.

References

Antolak, J. A., R. A. Boyd, and K. R. Hogstrom. (2002). "Evaluation of dosimetric issues related to IMET for a prototype EMLC." *Med. Phys*. 29:1285.

Antolak, J. A., G. Starkschall, E. R. Bawiec Jr., J. R. Ewton, and K. R. Hogstrom. "Implementation of an Automated Electron Bolus Fabrication System for Conformal Electron Radiotherapy" in *XIth International Conference on the Use of Computers in Radiation Therapy*. A. R. Hounsell, J. M. Wilkinson, and P. C. Williams (eds.). Manchester, UK: Christie Hospital NHS Trust, pp. 162–163, 1994.

Åsell, M., S. Hyödynmaa, A. Gustafsson, and A. Brahme. (1997). "Optimization of 3D conformal electron beam therapy in inhomogeneous media by concomitant fluence and energy modulation." *Phys. Med. Biol*. 42:2083–2100.

Bawiec Jr., E. R., (1994). The Effects of Accuracy in Milling of Electron Bolus on Dose Delivery. The University of Texas Health Science Center at Houston (M.Sc. thesis).

Boyd, R. A., J. A. Antolak, and K. R. Hogstrom. (2002). "Dosimetric characterization of a prototype EMLC for fixed beam therapy." *Med. Phys*. 29:1285.

Brahme, A. (1987). "Design principles and clinical possibilities with a new generation of radiation therapy equipment. A review." *Acta Oncol.* 26:403–412.

Brahme, A. (1988). "Optimisation of stationary and moving beam radiation therapy techniques." *Radiother. Oncol*. 12:129–140.

Deng, J., M. C. Lee, and C.-M. Ma. (2002). "A Monte Carlo investigation of fluence profiles collimated by an electron specific MLC during beam delivery for modulated electron radiation therapy." *Med. Phys*. 29:2472–2483.

Ebert, M. A., and P. W. Hoban. (1997). "Possibilities for tailoring dose distributions through the manipulation of electron beam characteristics." *Phys. Med. Biol*. 42:2065–2081.

Fields, R. S., and K. R. Hogstrom. "Optimization of Electron-Photon Mixed Beam Planning" in *Proceedings of the Eight International Conference on the Use of Computers in Radiation Therapy*. Silver Spring, MD: IEEE Computer Society Press, pp. 248–254, 1984.

Hogstrom, K. R. "Clinical Electron Beam Dosimetry: Basic Dosimetry Data" in *Advances in Radiation Oncology Physics: Dosimetry, Treatment Planning and Brachytherapy*. J. A. Purdy (ed.). AAPM medical Physics Monograph No. 19. Proceedings of the AAPM 1990 Summer School. New York, NY: American Institute of Physics, pp. 390–429, 1992.

Hogstrom, K. R., and D. D. Leavitt. "Dosimetry of Arc Electron Therapy" in *Radiation Oncology Physics–1986*. J. G. Kereiakes, H. R. Elson, and C. G. Born (eds.). AAPM Medical Physics Monograph No. 15. Proceedings of the AAPM 1986 Summer School. New York, NY: American Institute of Physics, pp. 265–295, 1987.

Hogstrom, K. R., M. D. Mills, and P. R. Almond. (1981). "Electron beam dose calculations." *Phys. Med. Biol*. 26:445–459.

Hogstrom, K. R., R. G. Kurup, A. S. Shiu, and G. Starkschall. (1989). "A two-dimensional pencil-beam algorithm for calculation of arc electron dose distributions." *Phys. Med. Biol.* 34:315–341.

Holmes, T., and T. R. Mackie. (1994). "A filtered backprojection dose calculation method for inverse treatment planning." *Med. Phys*. 21:303–313.

Hyödynmaa, S., A. Gustafsson, and A. Brahme. (1996). "Optimization of conformal electron beam therapy using energy- and fluence-modulated beams." *Med. Phys*. 23:659–666.

Janssen, J. J., E. W. Korevaar, P. R. Storchi, and H. Huizenga. (1997). "Numerical calculation of energy deposition by high-energy electron beams: III-B. Improvements to the 6D phase space evolution model." *Phys. Med. Biol*. 42:1441–1449.

Jeraj, R., and P. Keall. (1999). "Monte Carlo-based inverse treatment planning." *Phys. Med. Biol*. 44:1885–1896.

Jiang, S. B., T. Pawlicki, and C.-M. Ma. (2000). "An aperture-based inverse planning algorithm for modulated electron radiation therapy." CD-ROM Proceedings of the World Congress on Medical Physics and Biomedical Engineering, July 23–28, 2000, Chicago, IL.

Jiang, S. B., T. Pawlicki, F. Gracia, T. Guerrero, M. C. Lee, J. S. Li, J. Deng, D. R. Goffinet, A. L. Boyer, and C.-M. Ma. (2000). "Modulated electron radiation therapy: A new treatment modality." *Int. J. Radiat. Oncol. Biol. Phys*. 48(3 Suppl 1):218.

Karlsson, M. G., and M. Karlsson. (2002). "Electron beam collimation with focused and curved leaf end MLCs—experimental verification of Monte Carlo optimized designs." *Med. Phys*. 29:631–637.

Karlsson, M. G., M. Karlsson, and C.-M. Ma. (1999). "Treatment head design for multileaf collimated high-energy electrons." *Med. Phys*. 26:2161–2167.

Karlsson, M. G., M. Karlsson, and B. Zackrisson. (1998). "Intensity modulation with electrons: calculations, measurements and clinical applications." *Phys. Med. Biol*. 43:1159–1169.

Khan, F. M., K. P. Doppke, K. R. Hogstrom, G. J. Kutcher, R. Nath, S. C. Prasad, J. A. Purdy, M. Rozenfeld, and B. L. Werner. (1991). "Clinical electron-beam dosimetry: Report of AAPM Radiation Therapy Committee Task Group No. 25." *Med. Phys*. 18:73–109. (Also available as AAPM Report No. 32.)

Klein, E. E. (1998). "Modulated electron beams using multi-segmented multileaf collimation." *Radiother. Oncol*. 48:307–311.

Kudchadker, R., J. A. Antolak, W. H. Morrison, and K. R. Hogstrom. (2002a). "Conformal head and neck radiotherapy using custom electron bolus." *Med. Phys.* 29:1337.

Kudchadker, R. J., K. R. Hogstrom, A. S. Garden, M. D. McNeese, R. A. Boyd, and J. A. Antolak. (2002b). "Electron conformal radiotherapy using bolus and intensity modulation." *Int. J. Radiat. Oncol. Biol. Phys.* 53:1023–1037.

Leavitt, D. D., J. R. Stewart, and L. Earley. (1990). "Improved dose homogeneity in electron arc therapy achieved by a multiple-energy technique." *Int. J. Radiat. Oncol. Biol. Phys.* 19:159–165.

Leavitt, D. D., J. R. Stewart, J. H. Moeller, and L. Earley. (1989a). "Optimization of electron arc therapy doses by multi-vane collimator control." *Int. J. Radiat. Oncol. Biol. Phys.* 16:489–496.

Leavitt, D. D., J. R. Stewart, J. H. Moeller, W. L. Lee, and G. A. Takach, Jr. (1989b). "Electron arc therapy: Design, implementation and evaluation of a dynamic multi-vane collimator system." *Int. J. Radiat. Oncol. Biol. Phys.* 17:1089–1094.

Lee, M. C., S. B. Jiang, and C.-M. Ma. (2000). "Monte Carlo and experimental investigations of multileaf collimated electron beams for modulated electron radiation therapy." *Med. Phys*. 27:2708–2718.

Lee, M. C., J. Deng, J. Li, S. B. Jiang, and C.-M. Ma. (2001). "Monte Carlo based treatment planning for modulated electron beam radiation therapy." *Phys. Med. Biol*. 46:2177–2199.

Li, J. G., S. S. Williams, D. R. Goffinet, A. L. Boyer, and L. Xing. (2000). "Breast-conserving radiation therapy using combined electron and intensity-modulated radiotherapy technique." *Radiother. Oncol*. 56:65–71.

Lief, E. P., A. Larsson, and J. L. Humm. (1996). "Electron dose profile shaping by modulation of a scanning elementary beam." *Med. Phys*. 23:33–44.

Low, D. A., and K. R. Hogstrom. (1994). "Determination of the relative linear collision stopping and linear scattering powers of electron bolus material." *Phys. Med. Biol*. 39:1063–1068.

Low, D. A., G. Starkschall, S. W. Bujnowski, L. L. Wang, and K. R. Hogstrom. (1992). "Electron bolus design for radiotherapy treatment planning: Bolus design algorithms." *Med. Phys*. 19:115–124.

Low, D. A., G. Starkschall, N. E. Sherman, S. W. Bujnowski, J. R. Ewton, and K. R. Hogstrom. (1995). "Computer-aided design and fabrication of an electron bolus for treatment of the paraspinal muscles." *Int. J. Radiat. Oncol. Biol. Phys*. 33:1127–1138.

Ma, C.-M., and S. B. Jiang. (1999). "Monte Carlo modelling of electron beams from medical accelerators." *Phys. Med. Biol*. 44:R157–189.

Ma, C.-M., S. B. Jiang, T. Pawlicki, E. Mok, J. S. Li, J. Deng, A. Kapur, B. Yi, M. C. Lee, G. Luxton, and A. L. Boyer. (1999a). "Energy- and intensity-modulated electron beams for the treatment of breast cancer." *Int. J. Radiat. Oncol. Biol. Phys*. 45(3 Suppl 1):165–166.

Ma, C.-M., E. Mok, A. Kapur, T. Pawlicki, D. Findley, S. Brain, K. Forster, and A. L. Boyer. (1999b). "Clinical implementation of a Monte Carlo treatment planning system." *Med. Phys.* 26:2133–2143.

Ma, C.-M., T. Pawlicki, S. B. Jiang, J. S. Li, J. Deng, E. Mok, A. Kapur, L. Xing, L. Ma, and A. L. Boyer. (2000a). "Monte Carlo verification of IMRT dose distributions from a commercial treatment planning optimization system." *Phys. Med. Biol*. 45:2483–2495.

Ma, C.-M., T. Pawlicki, M. C. Lee, S. B. Jiang, J. S. Li, J. Deng, B. Yi, E. Mok, and A. L. Boyer. (2000b). "Energy- and intensity-modulated electron beams for radiotherapy." *Phys. Med. Biol*. 45:2293–2311.

Ma, C.-M., M. Ding, J. S. Li, M. C. Lee, T. Pawlicki, and J. Deng. (2003). "A comparative dosimetric study on tangential photon beams, IMRT and MERT for breast cancer treatment." *Phys. Med. Biol*. Submitted.

Mackie, T. R., P. J. Reckwerdt, C. M. Wells, J. N. Yang, J. O. Deasy, M. Podgorsak, M. A. Holmes, D. W. O. Rogers, G. X. Ding, B. A. Faddegon, C.-M. Ma, A. F. Bielajew, and J. Cygler. "The OMEGA project: Comparison among EGS4 electron beam simulations, Fermi-Eyges calculations and dose measurements." *XIth International Conference on the Use of Computers in Radiation Therapy*. A. R. Hounsell, J. M. Wilkinson, and P. C. Williams (eds.). Manchester, UK: Christie Hospital NHS Trust, pp. 152–153, 1994.

McNeeley, S., J. S. Li, R. A. Price, L. Chen, M. Ding, E. Fourkal, and C.-M. Ma. (2001). "An electron specific MLC for modulated electron radiation therapy." *Med. Phys*. 29:1286.

Pawlicki, T., and C.-M. Ma. (2001). "Monte Carlo simulation for MLC-based intensity-modulated radiotherapy." *Med. Dosim*. 26:157–168.

Perkins, G. H., M. D. McNeese, J. A. Antolak, T. A. Buchholz, E. A. Strom, and K. R. Hogstrom. (2001). "A custom three-dimensional electron bolus technique for optimization of postmastectomy irradiation." *Int. J. Radiat. Oncol. Biol. Phys*. 51:1142–1151.

Siebers, J. V., P. J. Keall, J. O. Kim, and R. Mohan. (2002). "A method for photon beam Monte Carlo multileaf collimator particle transport." *Phys. Med. Biol*. 47:3225–3249.

Starkschall, G., S. W. Bujnowski, J. A. Antolak, L.-H. Wang, and K. R. Hogstrom. "Tools for 3-D electron-beam treatment planning." *XIth International Conference on the Use of Computers in Radiation Therapy*. A. R. Hounsell, J. M. Wilkinson, and P. C. Williams (eds.). Manchester, UK: Christie Hospital NHS Trust, pp. 126–127, 1994.

Starkschall, G., S. W. Bujnowski, L. L. Wang, A. S. Shiu, A. L. Boyer, G. E. Desobry, N. H. Wells, A. L. Baker, and K. R. Hogstrom. (1991a). "A full three-dimensional radiotherapy treatment planning system." *Med. Phys*. 18:647.

Starkschall, G., A. S. Shiu, S. W. Bujnowski, L. L. Wang, D. A. Low, and K. R. Hogstrom. (1991b). "Effect of dimensionality of heterogeneity corrections on the implementation of a three-dimensional electron pencil-beam algorithm." *Phys. Med. Biol*. 36:207–227.

Svatos, M. M., J. G. Rosenman, and L. J. Verhey. (2000). "Effectiveness of mixing electrons with intensity modulated photons for reduction of integral dose for a variety of tumors sizes and depths." *Int. J. Radiat. Oncol. Biol. Phys*. 48(3 Suppl 1):140–141.

Tapley, N. D. (ed.). *Clinical Applications of the Electron Beam*. New York, NY: John Wiley & Sons, Inc., 1976.

Tobler, M., and D. D. Leavitt. (1996). “Design and production of wax compensators for electron treatments of the chest wall.” *Med. Dosim*. 21:199–206.

Webb, S. (1989). “Optimisation of conformal radiotherapy dose distributions by simulated annealing.” [Erratum appears in *Phys. Med. Biol*. 1990, 35(2):297]. *Phys. Med. Biol*. 34:1349–1370.

Zackrisson, B., and M. Karlsson. (1996). “Matching of electron beams for conformal therapy of target volumes at moderate depths.” *Radiother. Oncol*. 39:261–270.